

Zero-temperature phase of the XY spin glass in two dimensions: Genetic embedded matching heuristic

Martin Weigel*

*Department of Mathematics and the Maxwell Institute for Mathematical Sciences,
Heriot-Watt University, Edinburgh, EH14 4AS, UK*

Michel J. P. Gingras†

*Department of Physics and Astronomy, University of Waterloo, Waterloo, Ontario, N2L 3G1, Canada
(Dated: April 28, 2008)*

For many real spin-glass materials, the Edwards-Anderson model with continuous-symmetry spins is more realistic than the rather better understood Ising variant. In principle, the nature of an occurring spin-glass phase in such systems might be inferred from an analysis of the zero-temperature properties. Unfortunately, with few exceptions, the problem of finding ground-state configurations is a non-polynomial problem computationally, such that efficient approximation algorithms are called for. Here, we employ the recently developed genetic embedded matching (GEM) heuristic to investigate the nature of the zero-temperature phase of the bimodal XY spin glass in two dimensions. We analyze bulk properties such as the asymptotic ground-state energy and the phase diagram of disorder strength vs. disorder concentration. For the case of a symmetric distribution of ferromagnetic and antiferromagnetic bonds, we find that the ground state of the model is unique up to a *global* $O(2)$ rotation of the spins. In particular, there are no extensive degeneracies in this model. The main focus of this work is on an investigation of the excitation spectrum as probed by changing the boundary conditions. Using appropriate finite-size scaling techniques, we consistently determine the stiffness of spin and chiral domain walls and the corresponding fractal dimensions. Most noteworthy, we find that the spin and chiral channels are characterized by two distinct stiffness exponents and, consequently, the system displays spin-chirality decoupling at large length scales. Results for the overlap distribution do not support the possibility of a multitude of thermodynamic pure states.

PACS numbers: 75.50.Lk, 64.60.Fr, 02.60.Pn

I. INTRODUCTION

The discovery of materials without magnetic ordering down to zero temperature, but with an unusual cusp in the non-linear magnetic susceptibility¹ indicating a transition to a magnetically frozen but random state, has prompted a theoretical effort spanning over thirty years and aimed at the understanding of the perplexing properties of these spin-glass systems^{2,3,4,5}. Albeit mostly driven by the theoreticians' hope to understand the peculiar behavior of such systems within the framework of statistical mechanics, the results of this research have found widespread application in seemingly rather distant fields such as the theory of associative memory⁶, models of the immune system⁷ or error correcting codes^{8,9}. Spin-glass science thus provides for a classical example of how research driven by curiosity rather than application can lead to unexpected progress in diverse research areas. The canonical case of a spin glass, i.e., a noble metal host doped with magnetic transition metal ions² is not of particular interest as a material apart from the peculiarity of its properties. In recent years, however, many new materials with possible spin-glass phases have been discovered in compounds with highly frustrating lattice structures¹⁰. The large degeneracy of the ground state arising from geometric frustration alone gives rise to a host of novel and exotic magnetic phases, including spin glasses¹¹, but also spin liquids^{12,13} and spin ices¹⁴.

Experimental evidence suggests that spin-glass like phenomena appear to lie at the heart of several (potentially) technologically important phenomena, such as high temperature superconductivity, colossal magnetoresistance, and the anomalous Hall effect.

Other than might be suspected from the pure volume of published research in the field^{2,5}, however, owed to the unwieldy nature of the problem, even some very basic questions such as the existence of a finite-temperature phase transition have in general remained unanswered to date⁵. Starting from the, by now, rather complete¹⁵ understanding of the unusually complex mean-field theory^{16,17,18} of the fully connected (infinite dimensional) Sherrington-Kirkpatrick¹⁹ (SK) model, recent research has focused on the case of finite-dimensional systems. For the nearest-neighbor $O(n)$ Edwards-Anderson (EA) model²⁰ with Hamiltonian

$$\mathcal{H} = - \sum_{\langle ij \rangle} J_{ij} \mathbf{S}_i \cdot \mathbf{S}_j, \quad (1)$$

which has been studied in most detail, most of the effort has been devoted to the discrete case of classical Ising spins ($n = 1$). Even for this simplest case some controversial questions, such as the existence of a glassy phase at finite-temperatures in three dimensions (3D), could only be definitely answered in very recent years⁵. In general, many features such as the generic structure of valleys and barriers in the free energy and, more generally, the question of whether spin glasses in finite dimensions behave

essentially alike or differently from the mean-field case remain poorly understood^{21,22}. Even the allegedly simplest case of the Ising spin glass in two dimensions (2D) remains a topic of lively research activity^{23,24,25,26,27}.

For most of the materials featuring glassy magnetic phases, however, continuous XY or Heisenberg spins certainly are a more accurate description than the Ising model of extreme anisotropy in spin space^{2,3,11}. From the perspective of condensed matter physics, much attention has been paid to the experimentally important case of weak, but frustrating impurities and the question of a resulting loss of collinear order. Isolated frustrating antiferromagnetic defects in an otherwise ferromagnetic system couple to each other via an effective dipolar interaction^{28,29}, but it remains an open question whether collinear order can be destroyed with an arbitrarily small concentration of sufficiently strong defect bonds, and what role is played by the spatial dimension^{30,31,32,33}. Such models are potentially relevant to the weakly doped copper-oxide parents of high- T_c superconductors^{33,34,35}, while periodically frustrated XY systems are models of Josephson junction arrays^{31,36,37,38}. For the strong disorder case of a spin glass with symmetric bond distribution, the question of whether there is a non-zero transition temperature (for either or both of the spin and chiral sectors) in 3D XY and Heisenberg EA models is currently (again) hotly debated^{39,40,41,42,43,44}.

For the SK model, the ordered phase is characterized by a breaking of the abstract replica symmetry⁴⁵, but the nature of symmetry breaking in the short range case is less clear. Starting out from an essential analogy with the behavior of the ferromagnet, a phenomenological droplet scaling theory for the effective coupling in spin glasses has been formulated^{46,47,48,49,50}. The surface (free) energy of droplet excitations of length L is assumed to scale as $\Delta E \sim L^{\theta_s}$, defining the spin stiffness exponent θ_s . Put into the context of a renormalization group (RG) framework⁴⁹, θ_s determines whether a system scales to weak coupling ($\theta_s < 0$) such that droplets can always destabilize the ordered phase, thus restricting its extension to zero temperature, or scales towards strong coupling ($\theta_s > 0$) such that large-scale excitations are sufficiently costly to allow for a stable spin-glass phase at finite temperatures $0 < T < T_{SG}$. In the infinite-range SK model, the notion of droplets is maldefined and, instead, it is found that excitations of arbitrary size can be invoked at *constant* energy^{16,17,18,45}. Consequently, if mean-field theory applies to low-dimensional spin glasses, low-energy excitations are of rather different nature implying, for instance, space filling domain walls²¹. Hence, an analysis of overlaps between ground and systematically excited states can in principle allow to distinguish between the droplet and mean-field pictures^{51,52}. A standard way of producing excitations is a change of boundary conditions (BCs), e.g. from periodic to antiperiodic, the energy difference between both configurations capturing the energy of a relative domain wall^{46,53}.

For the 2D Ising spin glass, domain-wall energies scale

with $\theta_s = -0.287(4)$ for Gaussian bond distribution⁵⁴ and $\theta_s = 0$ for bimodal couplings⁵⁵, and a true thermodynamic spin-glass phase occurs only at zero temperature in both cases. From the RG ansatz of Ref. 49, θ_s determines the divergence of the correlation length ξ as $T \rightarrow 0$ via $\nu = -1/\theta_s$, which is found to be consistent with finite-temperature Monte Carlo results for the Gaussian case^{23,56}. For the bimodal $\pm J$ distribution, on the other hand, the formal $\nu = \infty$ has been interpreted as *exponential* divergence²⁵ of ξ , but some evidence for an algebraic singularity has also been presented recently²⁶ (see also Ref. 57). For the case of continuous XY or Heisenberg spins, the situation is complicated by the fact that the non-collinear spin structure in the ordered phase allows for the distinction of proper and improper $O(n)$ transformations, such that the continuous $SO(n)$ rotational symmetry is augmented by a \mathbb{Z}_2 or Ising-like *chiral* symmetry related to the determinant of the $O(n)$ rotation matrix⁵⁸. It has been argued⁵⁹ that these chiral degrees-of-freedom might decouple from the rotational ordering, resulting in different transition temperatures (above the lower critical dimension) or, at least, an additional chiral stiffness exponent θ_c (for $T_{SG} = 0$). Such a scenario is — after a long-winded debate — now quite well established in some periodically frustrated magnets^{60,61,62}, but remains fervently debated for the case of spin glasses^{39,41,42,44,63}. For the 2D XY spin glass, neither has θ_s been determined consistently, with estimates ranging from⁶⁴ $\theta_s = -1.0$ to⁶⁵ $\theta_s = -0.4$, nor has the question of a possible spin-chirality decoupling been satisfactorily resolved^{65,66}.

Methodologically, the above uncertainties regarding the XY spin glass are related to various technical difficulties. Firstly, finding ground states of spin-glass model systems is a computationally hard problem, generically believed to require an effort growing exponentially with system size⁶⁷. The 2D Ising spin glass on planar graphs is the only non-trivial exception to this rule, being polynomial computationally⁶⁸, and allowing for the rather precise estimate of θ_s cited above. Thus, reliable spin-glass ground state computations depend in general on rather elaborate and specifically tailored approximation algorithms to treat reasonably sized systems. In this context, we use here the recently proposed “genetic embedded matching” (GEM) technique^{69,70} to investigate the zero-temperature properties of the 2D XY spin-glass model. For the Ising problem mentioned, due to the existence of rather pronounced finite-size effects⁷¹ relatively large system sizes turned out to be necessary for reliable estimates, e.g., of θ_s . Below, we will see how progress in accessing much larger system sizes using the GEM approach now allows for investigations where finite-size effects seem for the first time rather well controlled. Secondly, there is no full agreement as to how BCs should be chosen in order to precisely excite either spin or chiral defects^{65,72}. This is of particular concern here, given that strong corrections to scaling depending on the chosen set of BCs have been observed for the Ising case^{54,73}. Here, we systematically study a wide range of BCs and resolve

the boundary dependent corrections to scaling.

The rest of the paper is organized as follows. Section II briefly discusses the employed GEM technique and the technical set-up of the calculations. In Sec. III, we discuss the asymptotic ground-state energy and the spectrum of metastable states found in the GEM calculations, while Sec. IV reports on the properties of excitations induced by a change of BCs. In particular, spin and chiral stiffness exponents and the associated fractal dimensions of domain walls are determined. Some of these results already were reported in part in Ref. 69. Section V contains our results for the scaling of overlap distributions, and Sec. VI presents some results on the distribution of internal fields and the disorder strength vs. disorder concentration phase diagram of the 2D randomly frustrated XY magnet. Finally, Sec. VII contains our conclusions.

II. ALGORITHM AND TECHNICAL SET-UP

Zero-temperature properties might be inferred from the $T \rightarrow 0$ limit of finite-temperature calculations such as Monte Carlo simulations. The latter, however, suffer from severe slowing down as the $T = 0$ critical point is approached for this system, thus rendering the extrapolated results rather unreliable. Hence we chose, instead, to determine ground states directly from non-equilibrium methods. Apart from the 2D Ising EA model on planar graphs, such computations are believed (and in some cases proven) to be *NP* hard¹¹⁵ optimization problems⁶⁷. To make progress with the 2D XY model, we take inspiration from the approach making the 2D Ising EA model solvable⁶⁸. In particular, we *embed* Ising variables into the continuous XY spins: with respect to a random, but fixed direction \mathbf{r} in spin space, the $O(n)$ spins \mathbf{S}_i of (1) decompose as $\mathbf{S}_i = \mathbf{S}_i^{\parallel} + \mathbf{S}_i^{\perp} = (\mathbf{S}_i \cdot \mathbf{r})\mathbf{r} + \mathbf{S}_i^{\perp}$. This results in a decomposition of \mathcal{H} as $\mathcal{H} = \mathcal{H}^{r,\parallel} + \mathcal{H}^{r,\perp}$ with

$$\mathcal{H}^{r,\parallel} = - \sum_{\langle i,j \rangle} \tilde{J}_{ij}^r \epsilon_i^r \epsilon_j^r, \quad (2)$$

where $\epsilon_i^r = \text{sign}(\mathbf{S}_i \cdot \mathbf{r})$, and where the effective couplings \tilde{J}_{ij}^r are given by

$$\tilde{J}_{ij}^r = J_{ij} |\mathbf{S}_i \cdot \mathbf{r}| |\mathbf{S}_j \cdot \mathbf{r}|. \quad (3)$$

If now the original $O(n)$ rotations of the spins are restricted to reflections along the plane defined by \mathbf{r} , \tilde{J}_{ij}^r as well as $\mathcal{H}^{r,\perp}$ are easily seen to be invariant under such reflections of individual spins, whereas the ϵ_i^r change sign. Hence, for a given \mathbf{r} , $\mathcal{H}^{r,\parallel}$ in (2) takes on the form of an Ising model with effective Ising “spins” ϵ_i^r .

The tractability of the 2D Ising ground-state problem in polynomial time comes about via the transformation to a graph-theoretical formulation⁶⁸. It rests on a dualization of the model: define elementary plaquettes of the square lattices to be frustrated if one or three of their surrounding bonds are antiferromagnetic⁷⁴. For a given

spin configuration, mark dual bonds of the square lattice as “active” if the corresponding original bond is unsatisfied, i.e., if $J_{ij} S_i S_j < 0$. Then, from the very definition of a frustrated plaquette, the set of “active” (dual) bonds consists of individual chains which are either closed loops or open chains connecting pairs of frustrated plaquettes, and the total energy of \mathcal{H} in (1) is (up to a constant) identical to the total sum of J_{ij} along the “active” bonds. Since on a planar lattice closed loops can always be removed by contraction, a ground state of the spin system corresponds to a *minimum-weight perfect matching* of the frustrated plaquettes, i.e., a configuration of the active bonds matching up all pairs of frustrated plaquettes while minimizing the total weight $\sum J_{ij}$ of bonds contained. Such problems can be solved in polynomial time by means of Edmonds’ “blossom algorithm”⁷⁵, and, most importantly, the solution can be shown to always correspond to a valid spin configuration for the case of planar graphs⁶⁸. As a result, application of (anti-)periodic BCs is restricted to at most one direction to preserve planarity. See Refs. 67,68,70 for a more detailed account of the relation between the Ising ground state and graph-theoretical matching problems.

Using the decomposition (2) for the $O(n)$ Hamiltonian (1), the blossom algorithm can be used to find exact ground states of the embedded Ising spins ϵ_i^r , corresponding to a reflection of some of the continuous spins with respect to the plane defined by a randomly chosen direction \mathbf{r} . A random sequential sampling of directions \mathbf{r} is used to statistically recover the full $O(n)$ symmetry. This *embedded matching* procedure is a strictly downhill search which, however, due to its non-local nature originating from the exact ground-state computation for the embedded Ising spins, features far less metastable states than a zero-temperature quench with any local dynamics⁷⁶. Due to the dependence of the effective couplings \tilde{J}_{ij}^r of (3) on the configuration $\{\mathbf{S}_i\}$, the embedded matching dynamics normally drives the system into a (low-lying) metastable state instead of the true ground state.

To find true ground states, the above embedded matching must be supplemented by a complementary protocol. We do so by inserting the embedded matching (i.e., minimization technique) as an optimization component (subroutine) into a specially tailored *genetic algorithm*^{69,77}. Here, a whole population of candidate ground state configurations is being worked on, continuously undergoing an improvement process mimicking natural evolution, which allows for a very efficient exploration of the landscape of metastable states of the system:

- **Crossover:** a random pair of spin configurations is selected as “parent configurations” and locally rigid domains or clusters are exchanged at random between them to produce “offspring” (see also Sec. III B).
- **Mutation:** a small proportion of spins of either offspring are randomly perturbed.

- **Optimization:** both offspring are optimized using the embedded matching technique.
- **Selection:** each parent is replaced by the morphologically closer offspring in case the latter has a lower internal energy.

The most crucial step in this sequence is the “crossover” operation. Indeed, special attention must be paid to the way configurations are combined in the crossover to balance the need for “genetic” diversification with the preservation of the high optimization on short length scales already achieved at intermediate steps of the process. Statistical analyzes show that the above combination of techniques in this *genetic embedded matching* (GEM) approach allows for a reliable determination of ground states for 2D XY spin glass samples of up to about 30×30 spins with current computing resources¹¹⁶. The algorithmic details of the GEM technique are quite intricate. A presentation of those details here would detract from our main agenda, which is to focus, and report, on the *physical* properties of the ground state of the 2D XY spin glass. A full account of the algorithmic details of the GEM technique can be found in Ref. 70.

For specificity, we assume a bimodal distribution of the quenched random couplings J_{ij} of (1),

$$P(J_{ij}) = (1 - x) \delta(J_{ij} - J) + x \delta(J_{ij} + \lambda J), \quad (4)$$

where λ denotes the relative strength of the antiferromagnetic impurity bonds $J_{ij} = -\lambda J$ and x their concentration. Unless stated otherwise, we averaged with respect to the distribution (4) by taking 5 000 independent disorder realizations and concentrated on the symmetric point $x = 0.5$, $\lambda = 1$, deep in the spin-glass regime of model (1) with $P(J_{ij})$ from Eq. (4). All computations discussed here were performed on square lattices. Choosing the parameters of the GEM runs to arrive at true ground states with high reliability, the run-times for single ground-state computations on a single 2.8 GHz PentiumIV CPU are between a few seconds for the smallest lattice sizes up to about 8 hours for a 28×28 system. In total, production of the data presented here consumed the equivalent of about 80 years of single CPU time.

III. ENERGETIC PROPERTIES

A. Asymptotic ground-state energy

To determine the asymptotic ground-state energy, we performed a finite-size scaling analysis with systems of different BCs, namely open and open-periodic (as mentioned above, fully periodic boundaries are not accessible to the method due to the planarity constraint⁶⁸). We used $L \times L$ systems with linear dimensions $L = 6, 8, 10, 12, 16, 20, 24$, and 28 and with 5 000 disorder replica for each system size. We consider the average, size-dependent internal energy per spin, $e(L) = \langle E/N_0 \rangle_J$,

where $\langle \cdot \rangle_J$ denotes a disorder average and N_0 is the number of lattice sites. From generic finite-size scaling arguments⁷⁸, at a $T = 0$ critical point, $e(L)$ should scale as⁷⁹

$$e(L) - e_\infty \sim L^{-(d-\theta_s)}, \quad (5)$$

where d denotes the spatial dimension and $\theta_s = -1/\nu$ was assumed⁴⁹. As usual, corrections to this form can be either non-analytic, stemming from irrelevant operators, or analytic and proportional to L^{-k} , $k = 1, 2, \dots$, from non-linear scaling fields⁸⁰. From the ϵ -expansion of the Ising spin glass, the leading non-analytic correction is (to first order in $\epsilon = 6 - d$) found⁷⁹ to be proportional to L^{θ_s-6} , asymptotically clearly smaller than the leading analytic correction term. Assuming a similar behavior for continuous spins, we shall restrict ourselves to analytical corrections here. Then, the most general form would be

$$e(L) - e_\infty = AL^{-(d-\theta_s)} + BL^{-1} + CL^{-2} + DL^{-3} + \dots \quad (6)$$

We first consider the case of fully open boundaries. Noting that in this case the analytical corrections can be at least partly attributed to the presence of edges and corners (cf., e.g., Ref. 81), Campbell *et al.*⁷⁹ take a slightly different approach and, instead of using $e(L)$, consider the energy $e^{\text{bd}}(L)/2$ per *bond* as the fundamental property, making the following scaling ansatz,

$$e^{\text{bd}}(L) - e_\infty^{\text{bd}} = \mathcal{B}^*/L + \mathcal{C}^*/L^2, \quad (7)$$

with \mathcal{B}^* representing edge effects and \mathcal{C}^* accounting for corner corrections. No term proportional to $L^{-(d-\theta_s)}$ is included in Eq. (7) arguing that free boundaries do not force any domain walls into the system. Indeed, excellent agreement with the data is found under this assumption for the case of the Ising spin glass⁷⁹. Since $L e(L) = (L - 1) e^{\text{bd}}(L)$, the parameters of Eqs. (6) and (7) are related as $e_\infty = e_\infty^{\text{bd}}$, $B = \mathcal{B}^* - e_\infty^{\text{bd}}$, $C = \mathcal{C}^* - \mathcal{B}^*$, $D = -\mathcal{C}^*$, and $A = 0$. Note that this effectively reduces the number of fit parameters of the form (6) with $A = 0$ from four to three, the $1/L^3$ term merely being produced from the $1/L^2$ correction of (7) by the transformation from bonds to sites. A fit of the form (6) with $A = 0$ to our data for free boundaries yields $e_\infty = -1.5520(14)$ with good quality-of-fit $Q = 0.35$. Using \mathcal{B}^* and \mathcal{C}^* as free parameters, on the other hand, yields a very similar estimate $e_\infty = -1.55331(56)$ with $Q = 0.48$. This last fit is shown together with the data in the upper panel of Fig. 1. It is interesting to note that the resulting parameter estimates $\mathcal{B}^* = -0.375(17)$ and $\mathcal{C}^* = 0.059(98)$ are in fact rather close to the values $\mathcal{B}^* = -0.3205(9)$ and $\mathcal{C}^* = 0.042(3)$ found for the *Gaussian* 2D Ising case and much further away from the estimates $\mathcal{B}^* = -0.5492(20)$ and $\mathcal{C}^* = 0.506(18)$ for the *bimodal* Ising spin glass⁷⁹. This is consistent with the expectation that the continuity of the XY spins effectively smoothes out the discrete bimodal distribution of couplings J_{ij} as far as energetic defects are concerned.

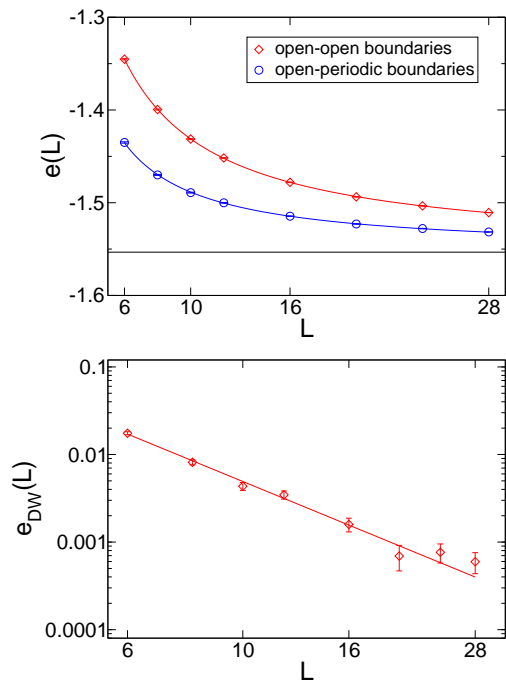


FIG. 1: (Color online) Top: Average ground-state energy per site for open-open and open-periodic boundaries. The fits are described in the main text, and the horizontal line shows the estimated asymptotic value of $e_\infty = -1.55331$. Bottom: domain-wall related correction to the internal energy for open-periodic BCs, which we denote by $e_{DW}(L)$, and which is given by $e_{DW}(L) = e(L) - e_\infty - (\mathcal{B}^* - e_\infty^{bd})/(2L) + \mathcal{B}^*/(4L^2)$. Here, the open-boundary estimates $e_\infty = -1.55331$ and $\mathcal{B}^* = -0.375$ have been used. The line shows a fit of the form $e_{DW}(L) = AL^{-(d-\theta_s)}$, yielding an estimate $\theta_s = -0.432(94)$.

For (mixed) open-periodic boundaries there is no reason to exclude an $L^{-(d-\theta_s)}$ term related to domain-wall trapping. In the scaling ansatz (7) for the bond energies, the $1/L^2$ correction should be omitted since the system has no corners, and the edge contribution should be cut in half. Since now $2Le(L) = (2L-1)e^{bd}(L)$, one identifies $B = (\mathcal{B}^* - e_\infty^{bd})/2$ and $C = -\mathcal{B}^*/4$. The statistical precision of the data is not sufficient to perform an unrestricted fit of the general form (6). Fixing $C = D = 0$ with the four unrestricted parameters e_∞ , A , θ_s and B remaining, we arrive at $e_\infty = -1.5525(13)$, $\theta_s = -0.49(69)$ and $Q = 0.35$. Fixing only $D = 0$, but reducing the number of parameters to four again by using the parametrization with \mathcal{B}^* and C^* yields a rather similar estimate $e_\infty = -1.5529(13)$, $\theta_s = -0.59(77)$ and $Q = 0.40$. Using the estimates $e_\infty = -1.55331(56)$ and $\mathcal{B}^* = -0.375(17)$ from the open-boundary case to reduce the number of parameters to two, on the other hand, yields a good fit ($Q = 0.38$) with a much more precise estimate $\theta_s = -0.432(94)$ (note, however, that the quoted statistical error does not take the uncertainty in the fixed parameters e_∞ and \mathcal{B}^* into account). This fit is displayed together with the data in the upper panel of Fig. 1. The lower panel shows the domain-wall related part $e_{DW}(L)$

of the energy correction for the open-periodic case. As is clearly seen, the domain-wall contribution is a very small correction to the internal energy. The estimate for θ_s is compatible with the result found from the domain-wall calculations for periodic BCs at fixed aspect-ratio $R = 1$ presented below in Sec. IV, but too large in modulus compared to our final estimate from the aspect-ratio scaling. One interesting question is whether spin and/or chiral defects should contribute to the domain-wall correction to the internal energy. We will show below in Sec. IV that the chiral defects are of much lower absolute energy for the considered lattice sizes than the spin defects, such that essentially only the spin defects are at play here, justifying post factum the interpretation of θ_s as the spin-stiffness exponent. Our best estimate for the asymptotic ground-state energy, $e_\infty = -1.55331(56)$, should be compared with the value $e_\infty = -1.40197(2)$ of the bimodal 2D Ising spin glass⁷⁹ which is, perhaps surprisingly, only about 10% higher. Hence, the enhanced ability of the continuous model compared to the discrete Ising case to locally adapt does not allow to substantially relieve the frustration imposed by the bond disorder (the unfrustrated system yielding, of course, $e_\infty = -2$).

B. Spectrum of metastable states

While a finely-tuned choice of parameters in the GEM approach guarantees high reliability for the optimization to arrive at a ground state, less optimal settings (in particular a reduction of the initial population size below a certain threshold) result in runs converging to low-lying metastable states instead^{69,70}. Additionally, and irrespective of the parameter choice, a part of the spectrum of low-lying metastable states appears as intermediate population members in the course of the optimization procedure. For a finite system this spectrum appears discrete¹¹⁷ (see below), and one naturally wonders what the nature of these excitations is. Comparing the configurations of some of these states, it is clearly seen that on short length scales the system is rigid within the space of energy minima, i.e., it naturally decomposes into stiff *clusters* of solidary spins whose individual moments have very similar orientations in all of the low-lying metastable states, apart from relative, essentially exact $O(n)$ rotations of whole clusters. Indications of such rigid clusters have been found in previous studies of Ising^{68,82} and continuous-spin systems^{66,83,84}. However, the genuine existence of such clusters for continuous spins had so far not been as well established numerically as we are able to achieve here with the GEM method. Note that such clusters are the finite-energy analogue of the “backbone” or “rigid lattice” of sites with constant relative spin orientation in all ground states observed in the $\pm J$ Ising spin glass with a large ground-state degeneracy⁸⁵. The GEM approach, and ultimately, its ability to determine the ground states, heavily relies on this cluster structure in the choice of operation for

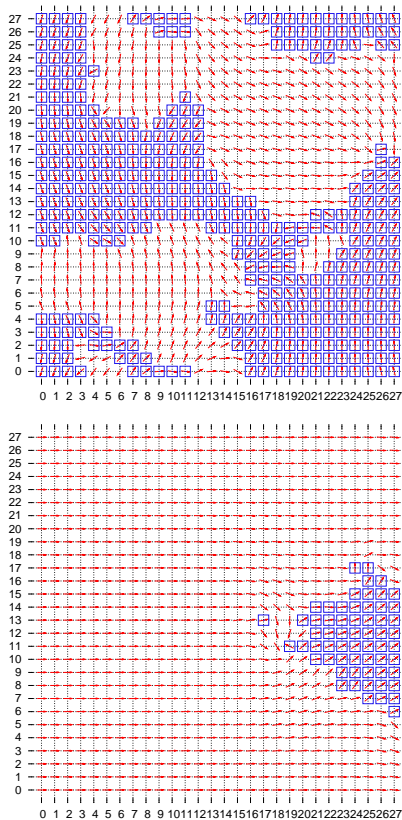


FIG. 2: (Color online) Local rotation matrices between the ground and first excited states for two 28×28 disorder realizations with open-periodic boundaries (periodic boundaries in the vertical direction). The arrows indicate the rotation angles, and blue squares are drawn in the case of improper rotations, i.e., negative determinant of the $O(2)$ matrix. See below in Sec. V for details about how these matrices are computed. The relative excitation energies are $\Delta E/E \approx 1.5 \times 10^{-5}$ (upper configuration) and $\Delta E/E \approx 2.4 \times 10^{-6}$ (lower configuration), respectively.

the crossover procedure exchanging such rigid domains between the “parent” replica, cf. the discussion in Sec. II and Ref.⁷⁰. As a result, the GEM algorithm effectively operates directly on the space of metastable states instead of on the whole of the continuous phase space⁷⁰. Products of independent $O(n)$ transformations of adjacent clusters (plus local excitations close to the boundaries between clusters) correspond to the domain-wall or droplet excitations postulated by the droplet theory of the spin glass phase^{48,49,50} and directly observed in Ising spin glasses^{50,55,71}. Finally, from the perspective of defect theory, the continuous symmetry of the order parameter also allows for *topological* excitations, here, according to the homotopy groups of $O(2)$, realized as domain-walls and vortex excitations⁸⁶. These can be explicitly observed in configurations^{70,83}, contributing to the thus rather rich variety of excitations appearing in this system.

Although a multitude of states with energies just

slightly above the ground state (with, e.g., $\Delta E/E$ as low as $\approx 10^{-6}$ for some 16×16 systems) is found, these energy differences are still far above the numerical resolution limits, and the configurations can be shown for each case to be truly different (see, for instance, the state differences depicted in Fig. 2). Naturally, each of these states has an $|O(n)|$ degeneracy corresponding to a global (proper or improper) rotation of all spins. Conversely, however, we checked for additional non-trivial degeneracies and found that statistically independent GEM runs always converged to an $O(n)$ rotated copy of the same state. Hence, the ground state of the system appears unique modulo the global symmetry. Consequently, quantities related to statistical fluctuations vanish at $T = 0$ and η , the exponent of the correlation function, is equal to zero⁴⁹. In terms of the clusters of rigid spins observed, the unique ground state results from the fact that the rigid clusters are not free, but their rigid $O(n)$ rotations have some non-vanishing excitation energy from necessary local adaptations of boundary spins.

By design, the GEM approach does not explicitly find *all* states of a given energy. In particular, as a non-equilibrium technique it does not find states with probabilities corresponding to their respective Boltzmann weights. However, there is no reason to believe that in all cases a single or possibly a multitude of degenerate ground states would dominate so strongly that not a single degenerate state appears in the thousands of independent runs undertaken. In contrast, the combined binary symmetry of the bimodal Ising spin glass results in a massive degeneracy of the ground state⁶⁸, such that already a typical 10×10 system has between 10^4 and 10^6 ground states⁸⁷. Monte Carlo simulations^{64,88} and Migdal-Kadanoff RG calculations⁸⁹ have led to speculations that the pairing of bimodal couplings with the discrete chiral symmetry might give rise to a similar situation in the bimodal XY spin-glass model considered here. Certainly, if calculations such as finite-temperature Monte Carlo simulations are sensitive to a (possibly narrow) *range* of energies, the observed dense spectrum of states might effectively appear as quasi-degenerate, resulting in an erroneously non-zero estimate of η from such simulations^{64,88}. Also, one might speculate about degeneracies in excited states which we have not investigated here, but might have shown up in some of the previous studies.

The low-lying metastable states appearing in the process of a GEM run might allow to learn something about the spectral properties of the system. Assuming a unique leading exponent in the scaling of defect energies with length scale, it is interesting to see how the lowest-energy excitations corresponding to the gap relate to the domain-wall or droplet excitations that are crucial for the understanding of the spin-glass phase. In Fig. 3 we show the gap energies for a series of $L \times 6L$ systems with open-periodic BCs (the non-trivial aspect ratio is chosen to reduce corrections to scaling, see the discussion below in Sec. IV). A fit of the functional

form $\langle \Delta E_{\text{gap}} \rangle_J \sim L^{\theta_{\text{gap}}}$ to the data for $L \geq 5$ yields an estimate of $\theta_{\text{gap}} = -1.447(31)$. Thus, the energy gap closes rather rapidly, leading to the expected quasi-continuous spectrum of metastable states in the thermodynamic limit. Also, θ_{gap} is clearly far more negative than the estimate $\theta_s \approx -0.3$ of the spin-stiffness exponent found below in Sec. IV from the domain-wall energy scaling. In fact, the energies of domain walls induced by a change from periodic to antiperiodic boundaries, additionally shown in Fig. 3 for comparison, are much larger than the gap energies for the whole range of system sizes considered. It is thus clear (at least as far as the range of available finite lattice sizes allows to judge) that the excitations reflected in the gap scaling are *not* in general extended defects of the domain-wall type. If, as argued here, metastable states are related to the ground state by rigid $O(n)$ rotations of one or several clusters (plus certain local adaptations at the cluster boundaries), it appears that the gapped excitations correspond to rotations of single (or few) such clusters, resulting in a lower excess energy than observed from the larger number of clusters that recombine to form a domain-wall defect. This view is corroborated by the snapshots of defects corresponding to the differences between ground and first excited states depicted in Fig. 2. Besides the extended defects with sizes of order L which might as well be incurred by a change of BCs (upper panel in Fig. 2), in many cases much more localized defects, corresponding to single rigidly $O(n)$ rotated clusters, are the lowest excitations (lower panel in Fig. 2). These two situations (represented by the upper and lower panels of Fig 2) allow us to interpret the rapid drop of gap energies indicated by the estimate of θ_{gap} as the effect of an additional implicit condition of minimum energy. For a given disorder configuration, ΔE_{gap} is not the average energy cost incurred by the $O(n)$ rotation of a single cluster, but the minimum cost of all possible such rotations of clusters. Finally, it should be noted that ΔE_{gap} is naturally not confined to either spin or chiral^{58,59} sectors, such that depending on the disorder configuration spin or chiral defects make up the gapped excitation.

IV. DOMAIN WALLS

For a systematic determination of the spin and chiral stiffness exponents θ_s and θ_c , respectively, a controlled and direct insertion of the corresponding defects into the system is needed. This is most conveniently achieved by using an appropriate choice of BCs. Droplet excitations could be created by similar means^{71,90}, but we have not explored this yet.

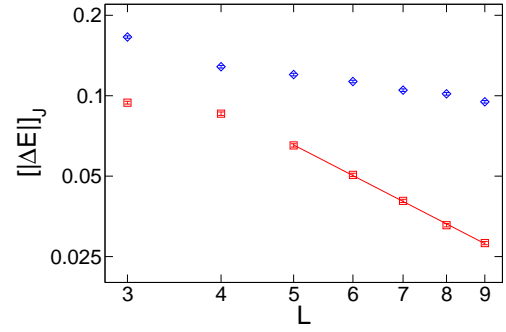


FIG. 3: (Color online) Scaling of the energy gap between ground state and lowest excited metastable state as estimated from the GEM approach for $L \times 6L$ systems with open-periodic BCs. The line shows a fit of the form $\langle \Delta E_{\text{gap}} \rangle_J \sim L^{\theta_{\text{gap}}}$ to the data. For comparison, the upper data set shows the average energy of domain walls induced by a change from periodic to antiperiodic BCs.

A. Choice and implementation of boundary conditions

For the Ising spin glass, defect energies are carried by domain walls or droplet surfaces which are the sharply localized boundaries of regions of inverted spins. For continuous symmetry, the notion of defects is more subtle since the spin direction varies smoothly, whereas chiralities are of the Ising type with localized boundaries (cf. Fig. 2). This is also seen in the types of topological defects allowed by the $O(n)$ symmetry, namely plain domain walls for the Ising case, but chiral domain walls *and* vortices for XY spins^{83,84,86}. The classic approach of measuring defect energies has been to analyze the difference between the energies E_P and E_{AP} of systems with periodic (P) and antiperiodic (AP) BCs⁵³. In contrast to a ferromagnet, however, both P and AP boundaries are in general frustrating for a spin glass such that, compared to the thermodynamic state, in a finite system domain walls or other defects are forced into the system. It is therefore not quite obvious what kind of excitation energy the difference $\Delta E_{P/AP}$ actually corresponds to. For the Ising case, the difference or sum of two domain-wall excitations is still essentially a linear excitation of length L , so one might expect to observe the scaling $|\Delta E|_{P/AP} \sim L^{\theta_s}$ predicted by droplet theory^{48,49}, which in fact turns out to work reasonably well for sufficiently large system sizes⁵. The continuous case with spin and chiral variables is less straightforward: the mere periodicity of periodic or antiperiodic BCs alone might force either spin or chiral excitations into the system, such that the interpretation of the difference $|\Delta E|_{P/AP}$ is rather unclear. While previously only P/AP boundaries (and the corresponding “reflective” boundaries for chiral defects) had been considered^{66,91,92}, Kosterlitz and Akino⁶⁵ suggested to alleviate the problem of trapped defects by additionally optimizing over a global twist angle along

the boundary and comparing the resulting configuration to one with a relatively π rotated or reflective boundary (“optimum twist” method). While such extra optimization over a global twist minimizes the frustrating effect of periodicity, it does not remove it, and hence spin and chiral defects remain incompletely disentangled.

A less ambiguous setup results from comparing the unrestricted, open-boundary system with the case of an explicitly inserted defect. We refer to this approach as open (O) and domain-wall (DW) BCs⁵⁵. The DW boundaries could be realized by fixing the spins along one of the two boundary seams under consideration in the positions of the O ground state and the spins of the other seam in a configuration rotated by π compared to the O state to induce a spin domain wall, cf. the sketch in Fig. 4. A fixing of spins is not possible within the GEM approach, however, since the spins do not have a direct representation in the dual matching problem. Instead, we link the boundary seams periodically with strong “anisotropic bonds” guaranteeing a fixed relative orientation of spins. In the embedded matching approach, for a pair $(\mathbf{S}_\mu, \mathbf{S}_\nu)$ of spins linked across the boundary, we choose an effective coupling

$$\tilde{J}_{\mu\nu}^r = J_{\text{strong}} \hat{\epsilon}_\mu^r \hat{\epsilon}_\nu^r \quad (8)$$

instead of the general embedded coupling (3). Here, $\hat{\epsilon}_\mu^r = \text{sign}(\hat{\mathbf{S}}'_\mu \cdot \mathbf{r})$, $\hat{\mathbf{S}}'_\mu = \mathcal{R}\hat{\mathbf{S}}_\mu$. The pair $(\hat{\mathbf{S}}_\mu, \hat{\mathbf{S}}_\nu)$ denotes the intended final relative orientation of $(\mathbf{S}_\mu, \mathbf{S}_\nu)$, i.e., in terms of the angles θ , $\mathbf{S} = (\cos \theta, \sin \theta)$, we have

$$\begin{aligned} \hat{\theta}_\mu - \hat{\theta}_\nu &= \theta_\mu - \theta_\nu + \pi & \text{for a spin DW,} \\ \hat{\theta}_\mu - \hat{\theta}_\nu &= \theta_\mu + \theta_\nu & \text{for a chiral DW.} \end{aligned} \quad (9)$$

Here, \mathcal{R} denotes a rigid rotation of the pair $(\hat{\mathbf{S}}_\mu, \hat{\mathbf{S}}_\nu)$ such that $\hat{\mathbf{S}}_\nu = \mathbf{S}_\nu$. In this way, any relative orientation $(\hat{\mathbf{S}}_\mu, \hat{\mathbf{S}}_\nu)$ can be forced upon the system by choosing a (non-random) $J_{\text{strong}} \gg \max |J_{ij}|$, such that a J_{strong} bond is never broken in an embedded matching run (for our computations, we chose $J_{\text{strong}} = 10^5$). The resulting excess contribution of the J_{strong} bonds is, of course, not counted in the final energy. For snapshots of excitations incurred by these O/DW spin and chiral boundaries, see Ref. 93. The prescription (9) for the chiral DW boundaries corresponds to a fixed axis of reflection independent of the disorder configuration (depending on the choice of origin for the angles θ_i). As an alternative, we have also considered a minimization procedure for the choice of the reflection axis. In particular, we chose the reflection axis perpendicular to the average direction of the boundary spins in order to minimize the boundary perturbation. We found very similar results to the case of the prescription of Eq. (9), such that it appears that this ambiguity does not have any bearing on the resulting value of the chiral stiffness exponent. For completeness, we also considered the standard P/AP BCs pair as well as random (R) and anti-random (AR) BCs pair, where the spins are fixed in random relative orientations using the procedure

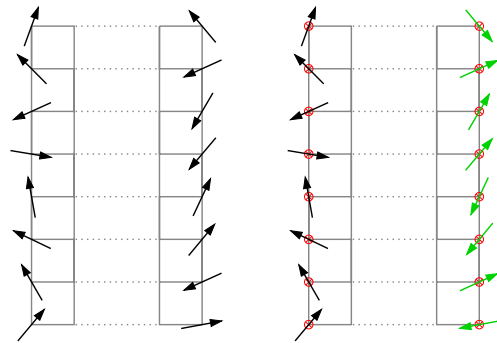


FIG. 4: (Color online) Open and domain-wall BCs. A ground state for open boundaries is determined, resulting in some configuration of the boundary spins (left). For spin domain-wall boundaries, the spins along the right boundary are then rotated by π and all boundary spins are held fixed for a second ground-state computation (right). In the actual implementation used, instead of locking the boundary spins, only their relative orientation is fixed.

described above for the R computation and in relatively π rotated orientations for the computations with AR BCs.

B. Spin and chiral stiffness

We have computed defect energies for $L = 6$ up to $L = 28$ systems with P/AP, R/AR and O/DW spin and chiral combinations of BCs. The results are collected in Fig. 5 together with fits of the form $\langle |\Delta E| \rangle_J \sim L^\theta$ to the data. Alternatively, one might consider the scaling of the width $\sigma(E) = \sqrt{\langle (\Delta E - \langle \Delta E \rangle_J)^2 \rangle_J}$, which leads to very similar results, and the final estimates of this approach will be discussed below. For the P/AP combination, a pronounced crossover is observed from the sizes $L \leq 12$ with $\theta_s = -0.724(21)$ to $\theta_s = -0.433(26)$ for $L \geq 16$. $L = 12$ was about the maximum size considered in previous studies^{65,66}, and our estimate for $L \leq 12$ is indeed consistent with these previous results as illustrated by the P/AP data of Ref. 65 shown for comparison. The result for $L \geq 16$, on the other hand, is much smaller in modulus and close to the value of $\theta_s \approx -0.4$ resulting from the “optimum twist” prescription of Ref. 65, indicating that it indeed reduces finite-size corrections to scaling. We note that the apparent crossover length $L \approx 12$ is comparable to the length below which no metastability occurs and the system behaves like a spherical spin glass^{91,94}. The scaling of defect energies for the R/AR combination of boundaries behaves quite similar to the P/AP case (as they are still periodic in nature), resulting in $\theta_s = -0.519(30)$ for somewhat smaller systems. The O/DW setup, on the other hand, not hampered by the periodicity effect, yields an even less negative estimate $\theta_s = -0.207(12)$. Finally, for the chiral defects, we find $\theta_c = -0.090(23)$.

As is seen from the variation of estimates with system size as well as between BCs, corrections to scaling are

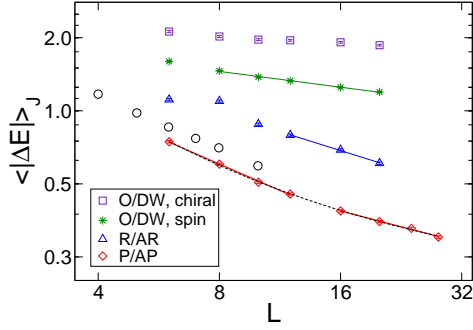


FIG. 5: (Color online) Average defect energies $\langle |\Delta E| \rangle_J$ for four sets of BCs on square lattices as a function of system size L . The straight lines are fits of the form $\langle |\Delta E| \rangle_J \sim L^\theta$ to the data. The open black circles show the “random twist” result of Ref. 65 for comparison. The dashed line shows a fit of the form (10) with $C = D = 0$ to the P/AP data. Some data sets have been shifted vertically for better distinction.

strong. A very similar situation occurs for the Ising spin glass⁵⁴. On general grounds⁷⁸, we expect analytic and non-analytic finite-size scaling corrections,

$$\langle |\Delta E| \rangle_J(L) = AL^\theta(1 + BL^{-\omega}) + C/L + D/L^2 + \dots \quad (10)$$

In contrast to the scaling (6) of the internal energy, where the edge and corner effects were important, the dominant term is here given by the non-analytic correction which is connected to interactions as well as self-interactions of domain walls⁷¹. Due to the limited precision of the data, we have to set $C = D = 0$. We find that only for the P/AP case are corrections pronounced enough and a sufficient number of system sizes is available for a stable fit that includes a non-analytic $L^{-\omega}$ correction term. For this case (including all data points $L = 6, \dots, 28$), we arrive at $\theta_s = -0.18(27)$, $\omega = 1.21(28)$ with $Q = 0.43$ (cf. the dashed black curve in Fig. 5), whereas a fit including all data without the correction term (i.e., additionally setting $B = 0$) yields an unacceptable quality-of-fit $Q = 6 \times 10^{-16}$. Hence, including corrections to scaling seems, in principle, able to reconcile the data from different sets of boundaries. However, this can only be done at the expense of mounting statistical uncertainties which cannot be afforded for useful estimates with the available level of accuracy and range of system sizes.

As an alternative systematic treatment of scaling corrections for domain-wall calculations, it has been suggested to consider $L \times M$ systems with variable aspect ratios $R \equiv M/L$ (with the change of BCs occurring along the edges of length L)⁷³. In general, scaling depends on the aspect ratio⁷⁸, so we can write

$$\langle |\Delta E| \rangle_J(L) = L^\theta F(R), \quad (11)$$

with some scaling function $F(R)$. In the extreme case of very elongated systems, $R \rightarrow \infty$, one should approach the behavior of the one-dimensional (1D) system. For the 1D Ising model, it is found that $\langle |\Delta E| \rangle_J(L) \sim 1/M$

independent of BCs⁴⁹. For the XY symmetry, the situation is more involved due to the simultaneous presence of spin and chiral variables. It appears that there are distinct exponents $\theta = (d - 2) = -1$ related to spin waves and $\theta \approx -1.9$ related to chiral excitations for the (quasi) one-dimensional XY spin glass^{72,95}. We are not aware, however, of any tests of universality with respect to different BCs probing the same excitations in this model. However, it is clear that the influence of the boundaries must diminish for $R \gg 1$ as the average distance to the boundaries with variable conditions increases. To test this hypothesis, we performed additional GEM computations for systems with aspect ratios $R = 2$ and $R = 6$ with sizes $L = 4, 6, \dots, 16$ ($R = 2$) resp. $L = 3, 4, \dots, 9$ ($R = 6$) and 5000 disorder replica per lattice. In Fig. 6 we present the results for domain-wall energies as a function of system size L at aspect ratio $R = 6$. As is apparent, the slopes of the data for boundaries probing spin excitations, i.e., P/AP, R/AR and O/DW spin boundary conditions, are quite compatible with each other asymptotically, whereas energies of chiral domain walls decay considerably slower. If, as it hence appears, there is independence of BCs as $R \rightarrow \infty$, one expects scaling corrections depending on boundaries to gradually disappear as more and more elongated systems are being considered. For the Ising case, it was observed that to good approximation this limit is attained as^{54,73}

$$\theta(R) = \theta(R = \infty) + A_R/R. \quad (12)$$

Our estimates of $\theta(R)$ for the data at aspect ratios $R = 1, 2$ and 6 for the different sets of boundary conditions are presented in Fig. 7 together with fits of the form (12) to the data, also including the alternative scaling of the width $\sigma(E)$. For each aspect ratio, corrections at fixed R were taken into account by omission of points from the small- L side for the fits of the form (10) instead of including any correction terms (i.e., we set $B = C = D = 0$), cf. the fits presented in Fig. 6. In particular, data points were successively omitted from the small- L side until a satisfactory quality-of-fit Q was achieved. We indeed find a clear convergence of the P/AP, R/AR and O/DW spin stiffness exponents as more elongated systems are considered, indicating independence of BCs in this limit. We collect the extrapolated estimates in Table I, finding them all well compatible within statistical errors. As our final estimate we cite the weighted mean $\theta_s = -0.329(14)$ (we do not include the $\sigma(E)$ results in the average since they are not statistically independent). The chiral stiffness exponent θ_c , on the other hand, seems to be almost independent of the aspect ratio (at least as far as the scaling of the difference $|\Delta E|$ is concerned) with an asymptotic value of $\theta_c(R = \infty) = -0.114(16)$, clearly different from the value found for the spin stiffness, indicating spin-chirality decoupling in this model.

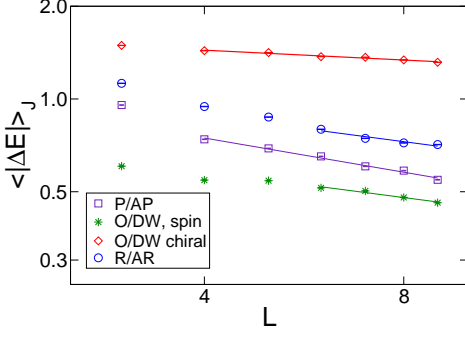


FIG. 6: (Color online) Scaling of average defect energies $\langle |\Delta E| \rangle_J$ for four sets of BCs at aspect ratio $R = 6$. The straight lines are fits of the form $\langle |\Delta E| \rangle_J \sim L^\theta$ to the data. Data sets have been shifted vertically for better distinction.

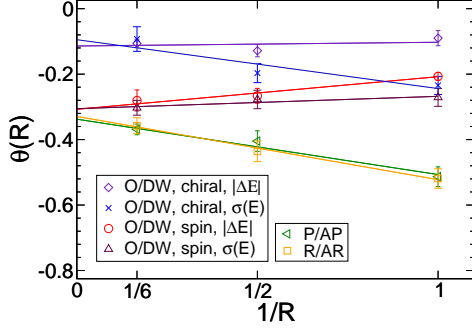


FIG. 7: (Color online) Dependence of the stiffness exponents θ_s and θ_c on the aspect ratio R of the systems for different pairs of BCs. The solid lines show fits of the form (12).

C. Domain-wall fractal dimension

On general grounds, the domain walls or droplet surfaces of the Ising spin glass have been assumed to be meandering curves with a non-trivial fractal dimension d_s (see Refs. 50,96). Measurements for the case of the 2D Ising spin glass with Gaussian interactions indeed yield a non-generic value⁹⁷ $d_s \approx 1.27$, and for the bimodal distribution quite similar estimates are found^{98,99,100}. A similar value has also been found in two-dimensional $O(n)$ spin glasses with additional random (off-diagonal) anisotropy¹⁰¹, which are expected to belong to the Ising spin-glass universality class¹⁰². The fractal dimension of domain walls is relevant to the question of whether the mean-field scenario, which predicts space-filling domain walls, i.e., $d_s = d$, applies to low dimensions²¹. Consider the link overlap,

$$q_l^{AB} = \frac{1}{N_1} \sum_{\langle i,j \rangle} (\mathbf{s}_i^A \cdot \mathbf{s}_j^A) (\mathbf{s}_i^B \cdot \mathbf{s}_j^B), \quad (13)$$

where N_1 denotes the number of bonds of the lattice, and the superscripts A and B stand for two replica of the system, here for the two BCs for a system with a

Boundaries	$ \Delta E $	$\sigma(E)$
P/AP	-0.338(20)	-0.348(19)
R/AR	-0.329(28)	-0.346(13)
O/DW spin	-0.308(30)	-0.306(26)
O/DW chiral	-0.114(16)	-0.095(38)

TABLE I: Spin and chiral stiffness exponents $\theta(R = \infty)$ from different sets of BCs as extrapolated via aspect-ratio scaling according to (12) for $|\Delta E|$ and the width $\sigma(E)$.

given realization of the random bonds. For the Ising case, bonds crossed by the domain wall contribute -1 to q_l^{AB} and all the others $+1$, such that

$$\langle 1 - q_l^{AB} \rangle_J \sim L^{-(d-d_s)}, \quad (14)$$

which allows to determine d_s numerically⁹⁷. The authors of Ref. 103 used the same relation for continuous spins (extrapolating from finite temperatures to $T = 0$). Due to the continuous nature of the spin response to the perturbation on the boundary, however, *all* spins contribute here to the reduction of q_l^{AB} and it is therefore almost inevitable that $\langle 1 - q_l^{AB} \rangle_J \sim L^0$, implying $d_s = d$. (It is likely that the small difference $d - d_s$ found by the authors of Ref. 103 is an artefact of the extrapolation from finite temperatures.) Here, we indeed find, e.g., $d - d_s = 0.0010(14)$ for the P/AP case and similar results for the other boundary conditions. Due to the above argument, however, this should not be seen as evidence for space-filling domain walls, but rather as an indicator for the inadequacy of the method.

As discussed above, domain walls in the system consist of the union of boundaries of rigidly $O(n)$ rotated clusters. To reveal this structure in the ground states identified, firstly one should get rid of the *global* symmetry by rigidly $O(n)$ rotating one configuration such as to maximize the total overlap $\hat{q}^{AB} = \sum_{\alpha,\beta} q_{\alpha\beta}^{AB} R_{\alpha\beta}^{AB}$, where $R_{\alpha\beta}^{AB}$ denotes the corresponding global rotation matrix, and

$$q_{\alpha\beta}^{AB} = \frac{1}{N_0} \sum_i S_{i\alpha}^A S_{i\beta}^B, \quad (15)$$

is the matrix of (site) overlaps. This is done by a singular value decomposition to diagonalize $q_{\alpha\beta}^{AB}$, in which case \hat{q}^{AB} is just the trace of the resulting diagonal $q_{\alpha\beta}^{AB}$, see Ref. 83. We refer to \hat{q}^{AB} as the “optimized” overlap (or projection) in contrast to the plain scalar overlap $q^{AB} = \sum_{\alpha} q_{\alpha\alpha}^{AB}$. Once this global symmetry has been removed, one can attempt to determine *local* rotation matrices to reveal rigid relative rotations of clusters of spins between the pair of configurations considered. To this end, we consider a locally averaged overlap matrix,

$$q_{\alpha\beta}^{AB}(\mathbf{x}) = Z(\mathbf{x})^{-1} \sum_i w(\mathbf{x}_i - \mathbf{x}) S_{i\alpha}^A S_{i\beta}^B, \quad (16)$$

where $Z(\mathbf{x}) = \sum_i w(\mathbf{x}_i - \mathbf{x})$, and $w(\mathbf{x}_i - \mathbf{x})$ is a rapidly decaying weighting function. The optimal local rotation

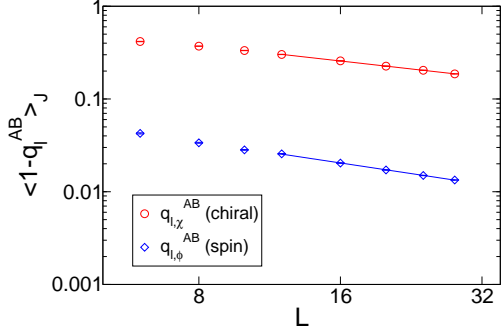


FIG. 8: (Color online) Scaling of the chiral link overlap $q_{l,\chi}^{AB}$ of Eq. (17) and the spin overlap $q_{l,\phi}^{AB}$ of Eq. (18) for $L \times L$ P/AP systems. The lines show fits of the functional form (14) to the data.

matrix $R_{\alpha\beta}^{AB}(\mathbf{x})$ again follows from a singular value decomposition. The averaging is necessary here since the comparison of a single pair of spins does not allow to uniquely determine an $O(2)$ matrix. In particular, one could not decide whether a proper or an improper rotation is involved. The weighting function $w(\mathbf{x}_i - \mathbf{x})$ is chosen exponentially decaying and cut off after two or three lattice spacings. The following results are independent of any fine-tuning of this falloff. The snapshots of Fig. 2 show the angles and signs of the thus determined rotation matrices $R_{\alpha\beta}^{AB}(\mathbf{x})$ (for snapshots of domain walls induced by a change of BCs, see also Ref. 93). Domain boundaries can be defined from $R_{\alpha\beta}^{AB}(\mathbf{x})$ separately for the spin and chiral parts: for the latter any bond with different signs of the determinant of $R_{\alpha\beta}^{AB}(\mathbf{x})$ at its two ends is crossed by a chiral domain wall, and for the former any bond with a change of the rotation angle ϕ of $R_{\alpha\beta}^{AB}(\mathbf{x})$ by more than a threshold value ϕ_0 is crossed by a spin domain wall. To determine d_s^χ for the chiral case, we define a link overlap analogous to (13),

$$q_{l,\chi}^{AB} = \frac{1}{N_1} \sum_{\langle i,j \rangle} [\det \mathbf{R}^{AB}(\mathbf{x}_i)] [\det \mathbf{R}^{AB}(\mathbf{x}_j)], \quad (17)$$

measuring the change in rotation signs along bonds. An analogous expression for $q_{l,\phi}^{AB}$ is used for d_s^ϕ of the spin domain walls,

$$q_{l,\phi}^{AB} = \frac{1}{N_1} \sum_{\langle i,j \rangle} \theta_{\phi_0}(\mathbf{x}_i, \mathbf{x}_j), \quad (18)$$

where $\theta_{\phi_0}(\mathbf{x}_i, \mathbf{x}_j) = -1$ if the angle between \mathbf{S}_i and \mathbf{S}_j exceeds ϕ_0 and $\det \mathbf{R}^{AB}(\mathbf{x}_i) = \det \mathbf{R}^{AB}(\mathbf{x}_j)$, and $\theta_{\phi_0}(\mathbf{x}_i, \mathbf{x}_j) = +1$ otherwise. Hence, bonds including a sign change of $\det \mathbf{R}^{AB}(\mathbf{x})$ are explicitly excluded from the counting to optimally decouple spin and chiral measurements. Fits of the form (14) are used to determine the corresponding fractal dimensions.

We consider the same sets of BCs and system sizes used for the determination of the stiffness exponents above.

Figure 8 shows the L dependence of the spin and chiral link overlaps $q_{l,\phi}^{AB}$ and $q_{l,\chi}^{AB}$, respectively, for the case of P/AP BCs and $L \times L$ systems, revealing clear scaling signals. For the chiral overlap, a fit of the form (14) to the data yields $d_s^\chi = 1.4291(44)$. The O/DW chiral boundaries presumably should show the clearest signal since direct visual inspection of the configurations reveals that typically a single domain wall roughly parallel to the variable boundary is excited. For this case we arrive at $d_s^\chi = 1.394(12)$. The sizable, although not dramatic, difference for the two choices of BCs shows that, as expected, still only partially controlled finite-size effects are present. Unfortunately, aspect-ratio scaling is not a suitable technique for the determination of d_s , at least for the system sizes accessible here: for the sizes $L = 3, \dots, 9$ of the $R = 6$ systems, the wall simply has no space to properly “meander” over the length of this couple of lattice spacings, resulting in very strong finite-size effects in L . Finally, as the third combination of boundaries considered, the O/DW spin boundary setup yields an extremely weak signal for the chiral domain walls since improperly $O(n)$ rotated domains occur only scarcely there, and we hence cannot produce a reliable estimate. We take the average of the P/AP and O/DW chiral results with sufficiently strong signals as our final estimate, $d_s^\chi = 1.425(12)$. The analysis of spin domain walls from the overlap $q_{l,\phi}^{AB}$ analogous to Eq. (17) is more involved due to the general dependence of the results on the cutoff angle ϕ_0 : if it is chosen too small, smooth rotations are counted as parts of domain boundaries, ultimately leading to space-filling domain walls in the limit $\phi_0 \rightarrow 0$. Choosing it too large, on the other hand, misses to recognize some of the cluster boundaries. We find somewhat stable results, however, in a range $0.5 \lesssim \phi_0 \lesssim 0.75$, and estimate $d_s^\phi = 1.2379(97)$ for P/AP and $d_s^\phi = 1.251(21)$ for O/DW spin boundaries. The O/DW chiral conditions yield too weak a signal for the determination of d_s^ϕ , and we again cite the average $d_s^\phi = 1.240(21)$ of the remaining two sets of boundaries as our best estimate. Thus, to the extent that finite-size corrections and the cutoff dependence of d_s^ϕ are under control, it appears that spin and chiral domain walls have different fractal properties.

V. OVERLAPS

One of the most striking results of the mean-field theory of the SK model is the occurrence of a multitude of pure states, resulting in a non-trivial distribution of the (thermally and disorder) averaged overlap parameter⁴⁵. Consequently, estimates of the form of the overlap distribution have been regularly considered as crucial benchmarks of the extent to which replica symmetry breaking occurs in finite-dimensional spin glasses⁵. In recent years it has become clear, however, that great care has to be taken when drawing conclusions from measurements on finite systems for the structure of pure states in spin

glasses^{21,51,104,105}. According to basic principles of statistical mechanics¹⁰⁶, a *thermodynamic state* should be defined as a limiting probability measure from a series of systems of increasing size, where a specific state is selected by an accompanying series of BCs. The resulting state is then identified by the values in this limit (if they exist) of all possible correlation functions in a central volume of the system, far away from the perturbing presence of the boundaries. If such a state cannot be decomposed into other thermodynamic states, i.e., it is mixed, it is termed pure. While this is rather clear in homogeneous systems such as ferromagnets, unfortunately, it is not known how a pure state should be explicitly constructed in spin-glass systems²¹. In particular, there is “chaotic size dependence” in such a sequence of system sizes resulting in oscillating and non-convergent correlation functions. It is also unknown how a convergent subsequence could be selected by coupling-independent BCs. It is clear, then, that considering the overlap distribution in whole, finite systems is not an appropriate way to detect the presence of a multitude of pure states¹¹⁸. In particular, the presence of domain walls separating patches of pure state configurations in finite systems might lead to a non-trivial overlap distribution even if only a single class of pure states related by a global $O(n)$ transformation was to exist. If, on the other hand, spins in a volume far away from the boundaries always converge to the same configuration (up to a common rotation) as $L \rightarrow \infty$, independent of BCs, a multitude of nonequivalent and observable pure states would appear to be ruled out.

An asymptotic independence from BCs of spin configurations in central windows can be detected either in (window) overlap distributions or in the behavior of correlation functions. These approaches are essentially equivalent⁵¹. To see this, consider two spins S_i and S_j inside a window W containing $N_W = w^2$ spins (for simplicity we consider Ising spins first). The average squared difference in the two-point functions between two systems with different BCs labelled A and B ,

$$\Delta = \frac{1}{N_W^2} \sum_{i,j \in W} \langle [\langle S_i^A S_j^A \rangle_T - \langle S_i^B S_j^B \rangle_T]^2 \rangle_J, \quad (19)$$

by construction scales to zero at fixed window size w if and only if the two-point functions for all window spins agree for almost-every disorder configuration (here $\langle \cdot \rangle_T$ denotes a thermal and $\langle \cdot \rangle_J$ a disorder average). It is then easy to see that in terms of the optimized overlap \hat{q}^{AB} of window spins (which for the Ising case $n = 1$ is just $|\hat{q}^{AB}|$) this is equivalently written as

$$\Delta = \langle (\hat{q}^{AA})^2 + (\hat{q}^{BB})^2 - 2(\hat{q}^{AB})^2 \rangle_{T,J}. \quad (20)$$

For the case of our XY model with a unique state at $T = 0$, up to a global $O(n)$ rotation (see Sec. III B above), \hat{q}^{AA} and \hat{q}^{BB} are of course always unity. Higher order (even) correlation functions lead to similar expressions with higher moments of \hat{q}^{AB} , such that in the most general context, the vanishing of the difference $\Delta P^{AB}(\hat{q}) =$

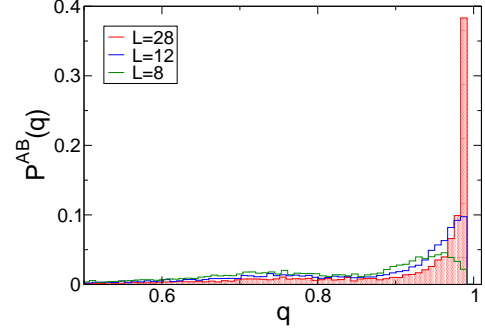


FIG. 9: (Color online) Sampled distribution of optimized overlaps \hat{q}^{AB} in central windows of size $w = 4$ for a change of BCs from periodic to antiperiodic. As the system size is increased, the distribution accumulates all its weight close to $\hat{q}^{AB} = 1$.

$P^{AA}(\hat{q}) + P^{BB}(\hat{q}) - 2P^{AB}(\hat{q})$ of overlap distribution functions is equivalent to the invariance of window correlation functions under a change of BCs. For the present case of non-degenerate ground states, this vanishing is attained only for the trivial form $P^{AB}(q) = \delta(q - 1)$, i.e., if and only if the window configurations are completely unchanged for almost every disorder configuration. A calculation along the same lines establishes the analogous relation between correlation functions and overlaps for the case of continuous spins.

We did not attempt to sample “all” BCs, but used the P/AP, R/AR and O/DW boundaries already considered for the defect-energy calculations. If the size w of the overlap window comes too close to the system size L , a crossover to the behavior of whole-system overlaps is seen, such that one strives to guarantee $w \ll L$. For too small windows, on the other hand, discretization or finite-size effects appear, and there is a certain probability that the two window configurations can be made to (almost) perfectly overlap by an $O(n)$ rotation although they are affected by the influence of the changed boundaries — down to the extreme case of $w = 1$ where *each* pair of configurations has $\hat{q}^{AB} = 1$. Thus, the intended behavior should appear for window sizes $1 \ll w \ll L$. As we shall show below, with available system sizes, these restrictions are best fulfilled for about $4 \lesssim w \lesssim 8$, but finite-size effects are still clearly visible due to the maximum $L \approx 28$ that we can reach with the GEM. In Fig. 9 we present the sampled distribution function of window overlaps \hat{q}^{AB} for the P/AP combination of BCs with $w = 4$, showing a clear tendency of statistical weight to accumulate at $\hat{q}^{AB} = 1$ as the system size L is increased, suggesting a convergence to the trivial form $P^{AB}(q) = \delta(q - 1)$ in the limit $L \rightarrow \infty$. The overlap distributions for the remaining pairs of BCs show a qualitatively similar behavior. For a more systematic study of this apparent convergence, we consider the total probability $p^{AB}(L, w)$ for the occurrence of an overlap \hat{q}^{AB} smaller than a threshold value \hat{q}_0 , measuring the distribution weight away from

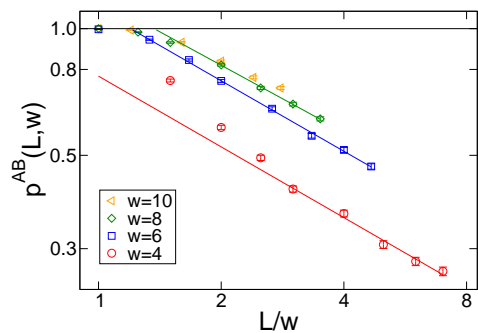


FIG. 10: (Color online) Scaling of the probability $p^{AB}(L, w)$ of an overlap $\hat{q}^{AB} < 0.9$ for the P/AP pair of BCs as a function of L/w . The lines show fits of the form (21) at fixed w to the data.

$\hat{q}^{AB} = 1$. To the extent to which the configurational changes induced by a change of BCs take the form of domain walls, this just measures the probability of the window being crossed by one of them. As discussed in Sec. IV C, such domain walls are fractal curves occupying a volume $\sim L^{d_s}$, such that a fraction of the lattice proportional to $L^{-(d-d_s)}$ will be touched by a domain wall (whether the relevant fractal dimension would rather be connected with spin or chiral defects will have to be decided post factum, see the discussion below). Since the relevant length scale in fact is L/w (remember that fractals are scale invariant), one expects an asymptotic scaling¹⁰⁴

$$p^{AB}(L, w) = Q_0(L/w)^{-(d-d_s)}. \quad (21)$$

Figure 10 shows the scaling of the crossing probability $p^{AB}(L, w)$ for $\hat{q}_0 = 0.9$ and the P/AP pair of BCs. We additionally considered cutoffs $\hat{q}_0 = 0.95$ and $\hat{q}_0 = 0.99$, changing the prefactor Q_0 of (21) and slightly modifying corrections, but yielding the same leading $(L/w)^{-(d-d_s)}$ behavior. There is a clear signal of scaling of $p^{AB}(L, w)$ to zero as the system size L is increased at fixed window size w . The expected collapse of data for different window sizes, however, only appears at $w \gtrsim 8$, at the edge of the window sizes that can be reasonably considered with the system sizes at hand. From fits to the scaling form (21) we find exponent estimates $d_s = 1.442(29)$, $d_s = 1.444(16)$ and $d_s = 1.472(21)$ for window sizes $w = 4$, $w = 6$ and $w = 8$, respectively. These are not only consistent with each other, but also compatible with the estimate $d_s^X = 1.425(12)$ found above for the fractal dimension of chiral domain walls. The remaining combinations of BCs yield rather similar results, with somewhat more pronounced finite-size corrections for the $L \leq 20$ systems considered there (in contrast to the aspect-ratio scaling of the domain-wall energies, where P/AP boundaries entailed the stronger corrections). In particular, we find $d_s = 1.404(17)$ from R/AR boundaries ($w = 6$), $d_s = 1.491(28)$ from O/DW spin BCs ($w = 4$) and $d_s = 1.489(59)$ for the O/DW chiral combination

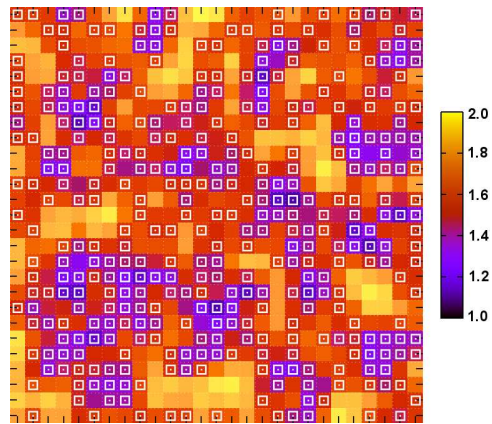


FIG. 11: (Color online) Spatial distribution of the internal field per link in the ground state of an example 28×28 disorder configuration with open-periodic BCs. There is a clear inverse correlation with the density of frustrated plaquettes (small white squares).

($w = 6$). It thus appears that the relevant domain walls seen in the window overlaps are of the chiral type. In total, clear signals of a scaling of the weight away from $\hat{q}^{AB} = 1$ to zero are seen in all cases, indicating a “deflection to infinity”²¹ of domain walls in the center of sufficiently large samples. The estimates for the fractal dimension seem to preclude an excitation of space-filling domain walls (i.e., $d_s = 2$) as predicted by a many-state picture at least from the coupling-independent and symmetric BCs considered. This is in agreement with the findings for the 2D Ising spin glass of Refs. 51,104.

VI. MAGNETIC PROPERTIES

A. Internal Fields

It is straightforwardly seen that a necessary condition for the Hamiltonian (1) to be in a metastable state is that each spin is parallel to its local internal field

$$\mathbf{h}_i^l = \frac{1}{q_i} \sum_j J_{ij} \mathbf{S}_j, \quad (22)$$

which for convenience has been normalized to represent the field *per link* by dividing by the local co-ordination number q_i , accounting for the difference in connectivity between spins along open boundaries and in the bulk. An iterative alignment of spin orientations along the internal field directions indeed drives the system towards a metastable (but not a ground) state, and the corresponding minimization technique is referred to as the Walker-Walstedt or spin-quench algorithm⁷⁶. The local strength of internal fields is closely linked to the presence of frustration in the system, with a weak internal field indicating a local uncertainty of the system with respect to choosing a given spin’s orientation such as to minimize the total energy. We indeed find a strong inverse

correlation between the size $|\mathbf{h}_i^l|$ of the internal fields in the ground state and the density of frustrated plaquettes of the system. This is illustrated for the ground state of an example disorder configuration of 28×28 spins in Fig. 11. It is clear that in terms of finding a ground state, optimal spin orientations in regions of low frustration (and consequently large internal fields) are rather easily determined, while it is much harder to optimize highly frustrated areas. This connection was exploited in the improved spin-quench method suggested in Ref. 32. One then also expects a certain correlation of the boundaries of rigid clusters discussed above in Sec. III and the occurrence of a high density of frustrated plaquettes.

Speculations on the occurrence of a certain proportion of sites with almost or exactly vanishing internal fields played some role in early models of the specific heat in spin glasses, see Ref. 76 and references therein. For the infinite-range case, it was subsequently established that $|\mathbf{h}_i^l| \geq h_0^l > 0$, such that (almost) free spins do not occur¹⁰⁷. For the short-range Heisenberg model, a similar exact bound was reported in Refs. 108,109. For the bimodal Ising spin glass, on the other hand, a multitude of flippable spins exists in each ground state¹¹⁰. For the intermediate XY case, however, to our knowledge no exact results are available. Figure 12 shows the distribution of internal fields $|\mathbf{h}^l|$ for 28×28 systems. Independent of BCs, no spins with fields $|\mathbf{h}^l| \lesssim 0.6 = h_0^l$ occur. Smaller systems have slightly larger gaps h_0^l , but the size dependence is very weak such that it is clear that a finite h_0^l survives in the thermodynamic limit. The absence of almost free spins in the ground state clearly illustrates the fact that there are no localized low-energy excitations and, instead, the lowest excitations are the extended defects corresponding to domain walls or $O(n)$ rotations of rigid clusters, as discussed in Sections III and IV. The distributions $P(|\mathbf{h}^l|)$ for the ground state show a characteristic behavior with the bulk of spins having $1.25 \leq |\mathbf{h}_i^l| \leq 1.75$ indicating strong frustration, but a certain number of almost fully satisfied spins leading to an extra peak close to $|\mathbf{h}_i^l| \approx 2$ associated to regions free of frustrated plaquettes. There are only small differences between the systems with open and periodic BCs, most noticeably a relative enlargement of this peak of unfrustrated spins for the open boundaries resulting from the relatively lower frustration of the extra boundary spins. For comparison, we also show the corresponding distribution for states found from the Walker-Walstedt zero-temperature quench, which asymptotically should result in an even sampling of *all* metastable states. This leads to a rather different distribution of internal fields where much less of the inherent frustration has been relieved. These curves for the finite-range model are markedly different from the distribution (again over all metastable states) of the infinite-range $O(2)$ SK model¹⁰⁷ shown for comparison which, due to the lack of local fluctuations in this infinite-dimensional model, is much more symmetric and more evenly frustrated.

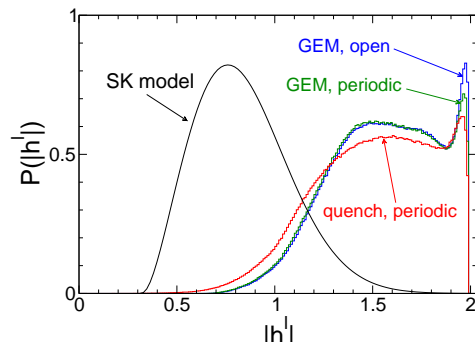


FIG. 12: (Color online) Average distribution of internal fields $|\mathbf{h}^l|$. The “GEM” curves represent ground states of 28×28 systems with open-open and open-periodic BCs. The “quench” data correspond to the average over a broad range of metastable states as found from the Walker-Walstedt algorithm⁷⁶. The curve labeled “SK model” shows the corresponding distribution in the $O(2)$ SK model¹⁰⁷.

B. Magnetic phase diagram

For small concentrations x and/or rather weak impurity bonds, one might expect the system to exhibit some rather extended short-range order³², or perhaps even long-range order³⁵, and from example calculations we indeed find clearly non-zero magnetizations for this region, whereas strongly disordered states of spin-glass signature appear once a larger number of strong impurity bonds is being introduced. Analytical calculations regarding the question of order and canting induced by impurity bonds have only been possible for isolated defects or using the mean-field type coherent potential approximation (CPA) of unclear precision for the case at hand^{29,30,31}. As a preliminary exploration of the zero-temperature phase diagram, we consider the modulus of the magnetization, $\langle |\mathbf{m}| \rangle_J$, where $\mathbf{m} = (\sum_i S_i)/N_0$. Figure 13 shows a contour plot of $\langle |\mathbf{m}| \rangle_J$ as a function of x and λ [cf. Eq. (4)] as found from GEM ground-state computations for systems of 16×16 spins and open BCs. Numerical calculations were actually performed at the grid of 30 points indicated by the tick marks in the plot, and the contours were produced from a 3rd order polynomial interpolation of the results. The bold black line indicates the locus of the curve $\langle |\mathbf{m}| \rangle_J = 0.5$ which could be used as a possible definition of a finite-size approximation of the phase transition line, approaching the true transition line as $L \rightarrow \infty$. The prediction of the CPA, namely³¹

$$x_c(\lambda) = \frac{1}{2} \frac{(1 - \sqrt{\lambda})^2}{1 + \lambda}, \quad (23)$$

is indicated by the bold white line. In the limit $\lambda \rightarrow 0$ of a diluted and unfrustrated system, order must disappear at the (bond) percolation threshold $x_c(\lambda = 0) = 0.5$ which is (by chance) already very well reproduced by the chosen definition $\langle |\mathbf{m}| \rangle_J = 0.5$ at the system size dis-

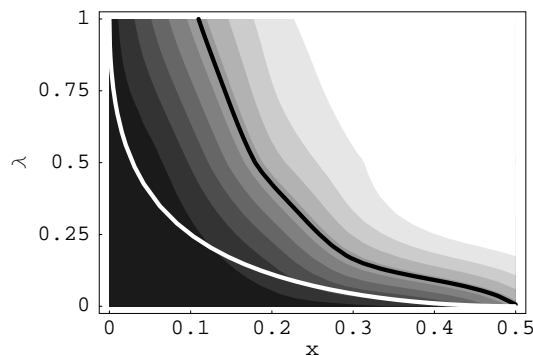


FIG. 13: Contour plot of the average ground-state magnetization $\langle |\mathbf{m}| \rangle_J$ for 16×16 systems with open BCs as a function of x and λ . Darker shades indicate larger magnetizations, and contours are separated by $\delta m = 0.1$. The bold black line denotes the locus of the curve $\langle |\mathbf{m}| \rangle_J = 0.5$, and the bold white line corresponds to the CPA prediction of Eq. (23).

played. Also, $x_c(0) = 1/2$ for the CPA form (23). There is no agreement in the literature about the general form of $x_c(\lambda)$ as $x \rightarrow 0$, i.e., in the experimentally most relevant regime of small dilution. According to (23), the CPA predicts a finite intercept $\lambda_c = 1$ for $x = 0$, and this claim was supported by the interpretation of the average magnetization found from a local spin-quench computation in Ref. 32 (at the same time, however, further results from the same study seemed to indicate the absence of long-range order for the whole phase diagram). An RG calculation for the non-linear σ model³³, on the other hand, appeared to indicate $\lambda_c \rightarrow \infty$ as $x \rightarrow 0$. The results of Fig. 13 certainly rather suggest that $\lambda_c > 1$ for $x \rightarrow 0$, but this impression might be distorted by finite-size effects. The question of long-range order is here rather subtle³¹, and it certainly cannot be excluded from the data shown that the indicated transition line is related to a crossover rather than a phase transition. In any case, this picture, of course, needs to change again at finite temperatures, where true long-range order is impossible due to the continuous symmetry of the system. A more thorough, finite-size scaling analysis of this question, together with an investigation into the nature of the apparently ordered phase (i.e., whether it is accompanied by transverse spin-glass order³²), is left as an interesting future application of the GEM technique.

VII. CONCLUSIONS

We have shown that a newly developed specially tailored heuristic optimization technique combining exact ground state computations for embedded Ising variables with a genetic algorithm allows for a thorough investigation of the ground state of the planar EA spin glass in two dimensions, contributing to a resolution of a number of long-standing issues for this system.

The main result consists of a careful determination of the spin and chiral stiffness exponents of the model with bimodal coupling distribution, which characterize its critical behavior and directly relate to the question of a possible spin-chirality decoupling in this system. In principle, a stiffness exponent related to domain walls can be extracted from scaling corrections to the finite-size behavior of the ground-state energy, but the precision of the estimate resulting from this method is not satisfactory. Instead, we investigated the properties of domain-wall defects directly induced by a suitable change of boundary conditions. In response to doubts regarding the suitability of the conventionally considered combination of periodic and antiperiodic boundary conditions resulting in an effective measurement of *differences* of defect energies⁶⁵, we explicitly excite domain-wall defects of the spin and chiral type relative to a system with free boundaries by applying special “domain-wall boundary conditions”. Corrections to scaling for these as well as for the additionally considered periodic-antiperiodic and random-antirandom boundaries are found to be large and their resolution, from explicitly including correction terms in fits to the defect energies, is not fully satisfactory given the accessible system sizes. However, application of the aspect-ratio scaling technique⁷³ allows for a good control over the boundary-dependent corrections, leading to a consistent estimate $\theta_s = -0.329(14)$ of the spin stiffness exponent for the different sets of boundary conditions used. This value is considerably smaller in modulus than the results of previous authors, quoting values of $\theta_s = -1.0$,⁶⁴ -0.9 ,⁹¹ -0.8 ,⁹² -0.78 ,⁶⁶ and $-0.37(2)$,⁶⁵ respectively. The spread of these previous results nicely illustrates the magnitude of present finite-size corrections as well as the hardness of computing true ground states for sufficiently large systems. The fact that in the present work, consistency between estimates of the stiffness exponent from different sets of boundary conditions with correction amplitudes of opposite signs could be achieved, makes it appear plausible that finally scaling corrections are under control to an acceptable degree of precision. Concerning the claim put forward in Ref. 65 that the P/AP combination of boundary conditions cannot be used to estimate the spin stiffness exponent, the results of the aspect-ratio scaling show that the assumed trapping of domain walls in periodic systems⁶⁵ only affects scaling corrections, but does not alter the asymptotic stiffness. This value of θ_s is remarkably close, but apparently not identical to the estimate $\theta_s = -0.287(4)$ found for the two-dimensional Ising spin glass with *Gaussian* coupling distribution⁵⁴. Also, scaling corrections to the ground state energy are found to be very close to the Gaussian Ising model, but rather different from the bimodal Ising spin glass. Chiral boundaries, on the other hand, lead to a clearly different exponent $\theta_c = -0.114(16)$, which is again remarkably smaller in modulus than previous estimates of $\theta_c = -0.6$,¹¹¹ -0.38 ,^{66,92} and $-0.37(1)$,⁶⁵ respectively. Consequently, it appears that spin and chiral degrees-of-freedom order with different exponents in

this system although, of course, a study for finite system sizes can never guarantee to probe the true asymptotic behavior. Naively, one might expect that the Ising-like chiral variables should lead to the value $\theta_c = 0$ of the bimodal Ising spin glass⁵⁵. It should be noted, however, that the chiral variables interact with an effective long-range Coulombic interaction⁵⁸, possibly leading to a shift in universality class. On the other hand, for the recently established spin-chirality decoupling in the periodically frustrated XY model^{61,62}, the chiral transition appears to show Onsager exponents, but this behavior is only seen for huge lattice sizes of $L \approx 10^3$, with wildly different behavior in the crossover region⁶². For our data, since for a θ_c very close to zero it becomes very hard numerically to distinguish the leading scaling from sub-leading corrections, we cannot definitely exclude the possibility of $\theta_c = 0$. In fact, including a finite asymptotic value ΔE_0 in the form (10) fits consistent with $\theta_c = 0$ can be achieved as well. In the context of the observed spin-chirality decoupling, it is therefore quite interesting that we find a θ_s value so close to that of the 2D Ising spin glass with Gaussian interactions.

We find that the structure of metastable states of the model can be understood in terms of metastates of clusters of rigidly locked spins, which undergo common relative $O(n)$ rotations between different metastable states. To each metastable state belongs a spectrum of continuous spin-wave excitations leaving the associated energy minimum. These will be considered in a future investigation. Low-energy excitations *within* the manifold of metastable states, on the other hand, are extended objects, corresponding to $O(n)$ rotations of one or several rigid clusters. Almost free spins corresponding to local excitations do not occur. Many such metastable configurations are found closely above the ground state, leading to a quasi-continuous spectrum in the thermodynamic limit. The ground states themselves, however, are found to be unique up to a global $O(n)$ transformation, implying a critical exponent $\eta = 0$ of the ground-state correlation function. Together with the estimates for θ_s and θ_c , this gives a rather complete characterization of the $T = 0$ critical point of the model.

We investigated the nature of elementary excitations induced by a change of boundary conditions by analyzing the locally averaged optimal rotation matrices between ground-state configurations. Chiral domain walls are by definition sharply localized. We find them to be fractal curves, and from the scaling of the corresponding link overlaps we estimate a fractal dimension $d_s^X = 1.425(12)$. The definition of spin domain walls depends on a somewhat arbitrary cutoff angle, but we find the fractal dimension $d_s^\phi = 1.240(21)$ to be independent of the cutoff within some reasonable range. Recently, evidence was presented for the hypothesis that domain walls in the Ising spin glass are special fractal curves described by “stochastic Loewner evolution” (SLE)^{112,113}. Compar-

ing the numerical results with conformal weights of the Kac table, the authors of Ref. 112 conjecture a relation $d_s = 1 + 3/4(3 + \theta)$. This we find fulfilled within statistical errors for d_s^ϕ , but not for the chiral exponent d_s^X where one might have rather expected it to hold. In any case, from the excitation via a change of boundary conditions, we do *not* find space-filling domain walls ($d_s = 2$) one necessarily expects for a model with many thermodynamic pure states²¹. This appears to be corroborated by an explicit investigation of the distribution of overlaps in central windows far away from the boundaries, which, for the system sizes accessible here, appears to converge to a trivial form $P^{AB}(\hat{q}) = \delta(\hat{q} - 1)$. This shows that the states defined by the considered set of boundary conditions always converge to the same class of thermodynamic pure states related by a global $O(n)$ rotation, and we do not find evidence for a multitude of pure states. Naturally, however, consideration of different types of boundary conditions might yield different results. The rate of this convergence is again related to a domain-wall fractal dimension, with a value compatible with d_s^X as determined directly.

A multitude of extensions of the present work comes to mind. Besides the mentioned investigation of spin-wave excitations complementing the information on metastable states presented here, certainly the magnetic phase diagram discussed in Sec. VI, which is relevant to a number of experimentally realized systems, deserves a more extensive investigation. Concerning the structure of the ground and excited states in terms of clusters of rigid spins, a more systematic analysis of the morphology along the lines of Refs. 85,114 appears promising. Clearly, investigations of Gaussian bond distributions and of the Heisenberg case would be highly interesting enterprises. Above all, however, the important question of spin-chirality decoupling in three-dimensional spin glasses could be tackled with a suitable generalization of the GEM approach employed here, replacing the embedded matching component inside the genetic algorithm by a technique applicable to three-dimensional systems.

Acknowledgments

The authors acknowledge fruitful discussions with I. Campbell. The research at the University of Waterloo was undertaken, in part, thanks to funding from the Canada Research Chairs Program (M.G., Tier 1), the Canada Foundation for Innovation and the Ontario Innovation Trust (M.G.). M.W. acknowledges support by the EC in form of a “Marie Curie Intra-European Fellowship” under contract No. MEIF-CT-2004-501422. This work was made possible, in part, by the facilities of the Shared Hierarchical Academic Research Computing Network (SHARCNET: www.sharcnet.ca).

-
- * Present address: Institut für Physik, Johannes-Gutenberg-Universität Mainz, Staudinger Weg 7, 55099 Mainz, Germany; Electronic address: weigel@uni-mainz.de
- † Electronic address: gingras@gandalf.uwaterloo.ca
- ¹ V. Cannella and J. A. Mydosh, Phys. Rev. B **6**, 4220 (1972).
 - ² K. Binder and A. P. Young, Rev. Mod. Phys. **58**, 801 (1986).
 - ³ K. H. Fischer and J. A. Hertz, *Spin Glasses* (University Press, Cambridge, 1991).
 - ⁴ A. P. Young, ed., *Spin Glasses and Random Fields* (World Scientific, Singapore, 1997).
 - ⁵ N. Kawashima and H. Rieger, in *Frustrated Spin Systems*, edited by H. T. Diep (World Scientific, Singapore, 2005), chap. 9, p. 491.
 - ⁶ H. Nishimori, *Statistical Physics of Spin Glasses and Information Processing* (Oxford University Press, Oxford, 2001).
 - ⁷ G. Parisi, Proc. Natl. Acad. Sci. USA **87**, 429 (1990).
 - ⁸ N. Sourlas, Nature **339**, 693 (1989).
 - ⁹ E. Dennis, A. Kitaev, A. Landahl, and J. Preskill, J. Math. Phys. **43**, 4452 (2002).
 - ¹⁰ J. E. Greedan, J. Mater. Chem. **11**, 37 (2001).
 - ¹¹ M. J. P. Gingras, C. V. Stager, N. P. Raju, B. D. Gaulin, and J. E. Greedan, Phys. Rev. Lett. **78**, 947 (1997).
 - ¹² J. S. Gardner, S. R. Dunsiger, B. D. Gaulin, M. J. P. Gingras, J. E. Greedan, R. F. Kiefl, M. D. Lumsden, W. A. MacFarlane, N. P. Raju, J. E. Sonier, et al., Phys. Rev. Lett. **82**, 1012 (1999).
 - ¹³ P. Mendels, F. Bert, M. A. de Vries, A. Olariu, A. Harrison, F. Duc, J. C. Trombe, J. S. Lord, A. Amato, and C. Baines, Phys. Rev. Lett. **98**, 077204 (2007).
 - ¹⁴ S. T. Bramwell and M. J.-P. Gingras, Science **294**, 1495 (2001).
 - ¹⁵ M. Talagrand, *Spin Glasses: Cavity and Mean Field Models* (Springer, Berlin, 2003).
 - ¹⁶ G. Parisi, Phys. Rev. Lett. **43**, 1754 (1979).
 - ¹⁷ G. Parisi, J. Phys. A **13**, 1101 (1980).
 - ¹⁸ G. Parisi, J. Phys. A **13**, 1887 (1980).
 - ¹⁹ D. Sherrington and S. Kirkpatrick, Phys. Rev. Lett. **35**, 1792 (1975).
 - ²⁰ S. F. Edwards and P. W. Anderson, J. Phys. F **5**, 965 (1975).
 - ²¹ C. M. Newman and D. L. Stein, J. Phys.: Condens. Matter **15**, R1319 (2003).
 - ²² P. Contucci, C. Giardinà, C. Giberti, G. Parisi, and C. Vernia, Phys. Rev. Lett. **99**, 057206 (2007).
 - ²³ H. G. Katzgraber, L. W. Lee, and A. P. Young, Phys. Rev. B **70**, 014417 (2004).
 - ²⁴ J. Lukic, A. Galluccio, E. Marinari, O. C. Martin, and G. Rinaldi, Phys. Rev. Lett. **92**, 117202 (2004).
 - ²⁵ H. G. Katzgraber and L. W. Lee, Phys. Rev. B **71**, 134404 (2005).
 - ²⁶ T. Jörg, J. Lukic, E. Marinari, and O. C. Martin, Phys. Rev. Lett. **96**, 237205 (2006).
 - ²⁷ R. Fisch, J. Stat. Phys. **125**, 789 (2006).
 - ²⁸ J. Villain, Z. Phys. B **33**, 31 (1979).
 - ²⁹ W. M. Saslow and G. N. Parker, Phys. Rev. B **38**, 11733 (1988).
 - ³⁰ G. N. Parker and W. M. Saslow, Phys. Rev. B **38**, 11718 (1988).
 - ³¹ J. Vannimenus, S. Kirkpatrick, F. D. M. Haldane, and C. Jayaprakash, Phys. Rev. B **39**, 4634 (1989).
 - ³² P. Gawiec and D. R. Grempel, Phys. Rev. B **44**, 2613 (1991).
 - ³³ F. Krüger and S. Scheidl, Phys. Rev. B **65**, 224502 (2002).
 - ³⁴ A. Aharony, R. J. Birgeneau, A. Coniglio, M. A. Kastner, and H. E. Stanley, Phys. Rev. Lett. **60**, 1330 (1988).
 - ³⁵ W. Y. Ching and D. L. Huber, Phys. Rev. B **42**, 493 (1990).
 - ³⁶ R. W. Reid, S. K. Bose, and B. Mitrović, J. Phys.: Condens. Matter **9**, 7141 (1997).
 - ³⁷ P. Gupta, S. Teitel, and M. J. P. Gingras, Phys. Rev. Lett. **80**, 105 (1998).
 - ³⁸ T. C. Halsey, Phys. Rev. Lett. **55**, 1018 (1985).
 - ³⁹ L. W. Lee and A. P. Young, Phys. Rev. Lett. **90**, 227203 (2003).
 - ⁴⁰ T. Yamamoto, T. Sugashima, and T. Nakamura, Phys. Rev. B **70**, 184417 (2004).
 - ⁴¹ K. Hukushima and H. Kawamura, Phys. Rev. B **72**, 144416 (2005).
 - ⁴² I. Campos, M. Cotallo-Aban, V. Martín-Mayor, S. Perez-Gaviro, and A. Tarancon, Phys. Rev. Lett. **97**, 217204 (2006).
 - ⁴³ T. Nakamura, Preprint cond-mat/0603062.
 - ⁴⁴ I. A. Campbell and H. Kawamura, Phys. Rev. Lett. **99**, 019701 (2007).
 - ⁴⁵ M. Mezard, G. Parisi, N. Sourlas, G. Toulouse, and M. Virasoro, J. Physique **45**, 843 (1984).
 - ⁴⁶ W. L. McMillan, Phys. Rev. B **29**, 4026 (1984).
 - ⁴⁷ A. J. Bray and M. A. Moore, J. Phys. C **17**, L463 (1984).
 - ⁴⁸ D. S. Fisher and D. A. Huse, Phys. Rev. Lett. **56**, 1601 (1986).
 - ⁴⁹ A. J. Bray and M. A. Moore, in *Heidelberg Colloquium on Glassy Dynamics*, edited by J. L. van Hemmen and I. Morgenstern (Springer, Heidelberg, 1987), p. 121.
 - ⁵⁰ D. S. Fisher and D. A. Huse, Phys. Rev. B **38**, 386 (1988).
 - ⁵¹ M. Palassini and A. P. Young, Phys. Rev. B **60**, R9919 (1999).
 - ⁵² E. Marinari and G. Parisi, Phys. Rev. B **62**, 11677 (2000).
 - ⁵³ J. R. Banavar and M. Cieplak, Phys. Rev. Lett. **48**, 832 (1982).
 - ⁵⁴ A. K. Hartmann, A. J. Bray, A. C. Carter, M. A. Moore, and A. P. Young, Phys. Rev. B **66**, 224401 (2002).
 - ⁵⁵ A. K. Hartmann and A. P. Young, Phys. Rev. B **64**, 180404(R) (2001).
 - ⁵⁶ J. Houdayer and A. K. Hartmann, Phys. Rev. B **70**, 014418 (2004).
 - ⁵⁷ R. Fisch, J. Stat. Phys. **128**, 1113 (2007).
 - ⁵⁸ J. Villain, J. Phys. C **10**, 4793 (1977).
 - ⁵⁹ H. Kawamura and M. Tanemura, Phys. Rev. B **36**, 7177 (1987).
 - ⁶⁰ D. Loison and P. Simon, Phys. Rev. B **61**, 6114 (2000).
 - ⁶¹ Y. Ozeki and N. Ito, Phys. Rev. B **68**, 054414 (2003).
 - ⁶² M. Hasenbusch, A. Pelissetto, and E. Vicari, J. Stat. Mech.: Theory and Exp. p. P12002 (2005).
 - ⁶³ H. Kawamura, J. Mag. Mag. Mater. **310**, 1487 (2007).
 - ⁶⁴ S. Jain and A. P. Young, J. Phys. C **19**, 3913 (1986).
 - ⁶⁵ J. M. Kosterlitz and N. Akino, Phys. Rev. Lett. **82**, 4094 (1999).
 - ⁶⁶ J. Maucourt and D. R. Grempel, Phys. Rev. Lett. **80**, 770 (1998).

- (1998).
- ⁶⁷ A. K. Hartmann and H. Rieger, *Optimization Algorithms in Physics* (Wiley, Berlin, 2002).
 - ⁶⁸ I. Bieche, R. Maynard, R. Rammal, and J. P. Uhry, *J. Phys. A* **13**, 2553 (1980).
 - ⁶⁹ M. Weigel and M. J. P. Gingras, *Phys. Rev. Lett.* **96**, 097206 (2006).
 - ⁷⁰ M. Weigel, Preprint arXiv:0706.4408, *Phys. Rev. E* (in print).
 - ⁷¹ A. K. Hartmann and M. A. Moore, *Phys. Rev. Lett.* **90**, 127201 (2003).
 - ⁷² T. Uda, H. Yoshino, and H. Kawamura, *Phys. Rev. B* **72**, 024442 (2005).
 - ⁷³ A. C. Carter, A. J. Bray, and M. A. Moore, *Phys. Rev. Lett.* **88**, 077201 (2002).
 - ⁷⁴ G. Toulouse, *Commun. Phys.* **2**, 115 (1977).
 - ⁷⁵ J. Edmonds, *J. Res. Natl. Bur. Stand. B* **69**, 125 (1965).
 - ⁷⁶ L. R. Walker and R. E. Walstedt, *Phys. Rev. B* **22**, 3816 (1980).
 - ⁷⁷ K. F. Pál, *Physica A* **223**, 283 (1996).
 - ⁷⁸ M. E. Barber, in *Phase Transitions and Critical Phenomena*, edited by C. Domb and J. L. Lebowitz (Academic Press, New York, 1983), vol. 8, p. 146.
 - ⁷⁹ I. A. Campbell, A. K. Hartmann, and H. G. Katzgraber, *Phys. Rev. B* **70**, 054429 (2004).
 - ⁸⁰ M. Henkel, *Conformal Invariance and Critical Phenomena* (Springer, Berlin/Heidelberg/New York, 1999).
 - ⁸¹ V. Privman, in *Finite Size Scaling and Numerical Simulation of Statistical Systems*, edited by V. Privman (World Scientific, Singapore, 1990), p. 1.
 - ⁸² G. Hed, A. K. Hartmann, D. Stauffer, and E. Domany, *Phys. Rev. Lett.* **86**, 3148 (2001).
 - ⁸³ C. L. Henley, *Ann. Phys. (NY)* **156**, 324 (1984).
 - ⁸⁴ C. L. Henley, *Ann. Phys. (NY)* **156**, 368 (1984).
 - ⁸⁵ F. Barahona, R. Maynard, R. Rammal, and J. P. Uhry, *J. Phys. A* **15**, 673 (1982).
 - ⁸⁶ G. Toulouse, *Phys. Rep.* **49**, 267 (1979).
 - ⁸⁷ J. W. Landry and S. N. Coppersmith, *Phys. Rev. B* **65**, 134404 (2002).
 - ⁸⁸ P. Ray and M. A. Moore, *Phys. Rev. B* **45**, 5361 (1992).
 - ⁸⁹ M. J. P. Gingras, *Phys. Rev. B* **46**, 14900 (1992).
 - ⁹⁰ N. Kawashima, *J. Phys. Soc. Jpn.* **69**, 987 (2000).
 - ⁹¹ B. W. Morris, S. G. Colborne, M. A. Moore, A. J. Bray, and J. Canisius, *J. Phys. C* **19**, 1157 (1986).
 - ⁹² H. Kawamura and M. Tanemura, *J. Phys. Soc. Jpn.* **60**, 608 (1991).
 - ⁹³ M. Weigel and M. J. P. Gingras, *J. Phys.: Condens. Matter* **19**, 145217 (2007).
 - ⁹⁴ L. W. Lee and A. P. Young, *Phys. Rev. E* **72**, 036124 (2005).
 - ⁹⁵ M. Ney-Nifle, H. J. Hilhorst, and M. A. Moore, *Phys. Rev. B* **48**, 10254 (1993).
 - ⁹⁶ A. J. Bray and M. A. Moore, *Phys. Rev. Lett.* **58**, 57 (1987).
 - ⁹⁷ A. K. Hartmann and A. P. Young, *Phys. Rev. B* **66**, 094419 (2002).
 - ⁹⁸ M. Weigel and D. A. Johnston, *Phys. Rev. B* **76**, 054408 (2007).
 - ⁹⁹ F. Romá, S. Risau-Gusman, A. J. Ramirez-Pastor, F. Nieto, and E. E. Vogel, *Phys. Rev. B* **75**, 020402(R) (2007).
 - ¹⁰⁰ O. Melchert and A. K. Hartmann, *Phys. Rev. B* **76**, 174411 (2007).
 - ¹⁰¹ M. J. P. Gingras, *Phys. Rev. Lett.* **71**, 1637 (1993).
 - ¹⁰² A. J. Bray and M. A. Moore, *J. Phys. C* **15**, 3897 (1982).
 - ¹⁰³ H. G. Katzgraber and A. P. Young, *Phys. Rev. B* **65**, 214401 (2002).
 - ¹⁰⁴ A. A. Middleton, *Phys. Rev. Lett.* **83**, 1672 (1999).
 - ¹⁰⁵ E. Marinari, G. Parisi, F. Ricci-Tersenghi, J. J. Ruiz-Lorenzo, and F. Zuliani, *J. Stat. Phys.* **98**, 973 (2000).
 - ¹⁰⁶ D. Ruelle, *Statistical Mechanics* (Benjamin, New York, 1969).
 - ¹⁰⁷ A. J. Bray and M. A. Moore, *J. Phys. C* **14**, 2629 (1981).
 - ¹⁰⁸ T. A. Kaplan and N. d'Ambrumenil, *J. Phys. C* **15**, 3769 (1982).
 - ¹⁰⁹ T. A. Kaplan and N. d'Ambrumenil, *J. Phys. C* **15**, 5535 (1982).
 - ¹¹⁰ A. K. Hartmann, *Phys. Rev. E* **63**, 016106 (2000).
 - ¹¹¹ H. S. Bokil and A. P. Young, *J. Phys. A* **29**, L89 (1996).
 - ¹¹² C. Amoruso, A. K. Hartmann, M. B. Hastings, and M. A. Moore, *Phys. Rev. Lett.* **97**, 267202 (2006).
 - ¹¹³ D. Bernard, P. Le Doussal, and A. A. Middleton, *Phys. Rev. B* **76**, 020403(R) (2007).
 - ¹¹⁴ F. Romá, S. Bustingorry, and P. M. Gleiser, *Phys. Rev. Lett.* **96**, 167205 (2006).
 - ¹¹⁵ For practical purposes, this means that although the penalty of a solution (i.e., here the energy of the spin configuration) can be computed in polynomial time, it is believed that there exists no algorithm for surely finding the optimal solution in polynomial time.
 - ¹¹⁶ Note that, although the embedded matching approach is polynomial, the XY ground-state problem itself is still NP -hard, such that, for instance, the population size in the genetic part needs to grow exponentially with system size at a constant success rate for finding ground states (see Ref. 70).
 - ¹¹⁷ Spin-wave excitations out of local minima do not occur in the set of these states because after each “optimization” step of the GEM the configuration is forced into the closest local minimum through a relaxational dynamics.
 - ¹¹⁸ Additionally, for the case of models without accidental degeneracies at $T = 0$, it is clear that the optimized overlap \hat{q}^{AB} is unity for each disorder configuration leading to a trivial overlap distribution $P^{AB}(q) = \delta(q - 1)$ and hence does not reveal any information about the structure of the general state space.